

1 **BIPV/T facades – a new opportunity for Integrated Collector-** 2 **Storage Solar Water Heaters?**

3 ***Part 1: State-of-the-art, theory and potential***

4
5 Adrian Pugsley^(a) (a.pugsley@ulster.ac.uk, +44(0)28 90366264 (corresponding author)
6 Aggelos Zacharopoulos^(a) (a.zacharopoulos@ulster.ac.uk) +44(0)28 90368227
7 Jayanta Deb Mondol^(a) (jd.mondol@ulster.ac.uk) +44(0)28 90368037
8 Mervyn Smyth^(a, b) (m.smyth1@ulster.ac.uk) +44(0)28 90368119

9 (a) *Centre for Sustainable Technologies* (www.cst.ulster.ac.uk), *School of the Built*
10 *Environment, Ulster University, Newtownabbey, BT37 0QB, Northern Ireland, UK*

11 (b) *SolaForm Ltd* (www.solaform.com) *c/o Ulster University, Newtownabbey, BT37 0QB,*
12 *Northern Ireland, UK*
13

14 **Keywords**

15 Integrated Collector-Storage Solar Water Heaters (ICSSWH); Photovoltaic-thermal
16 (PV/T); Thermal diode; building facade; solar collector; heat removal factor
17

18 **Highlights**

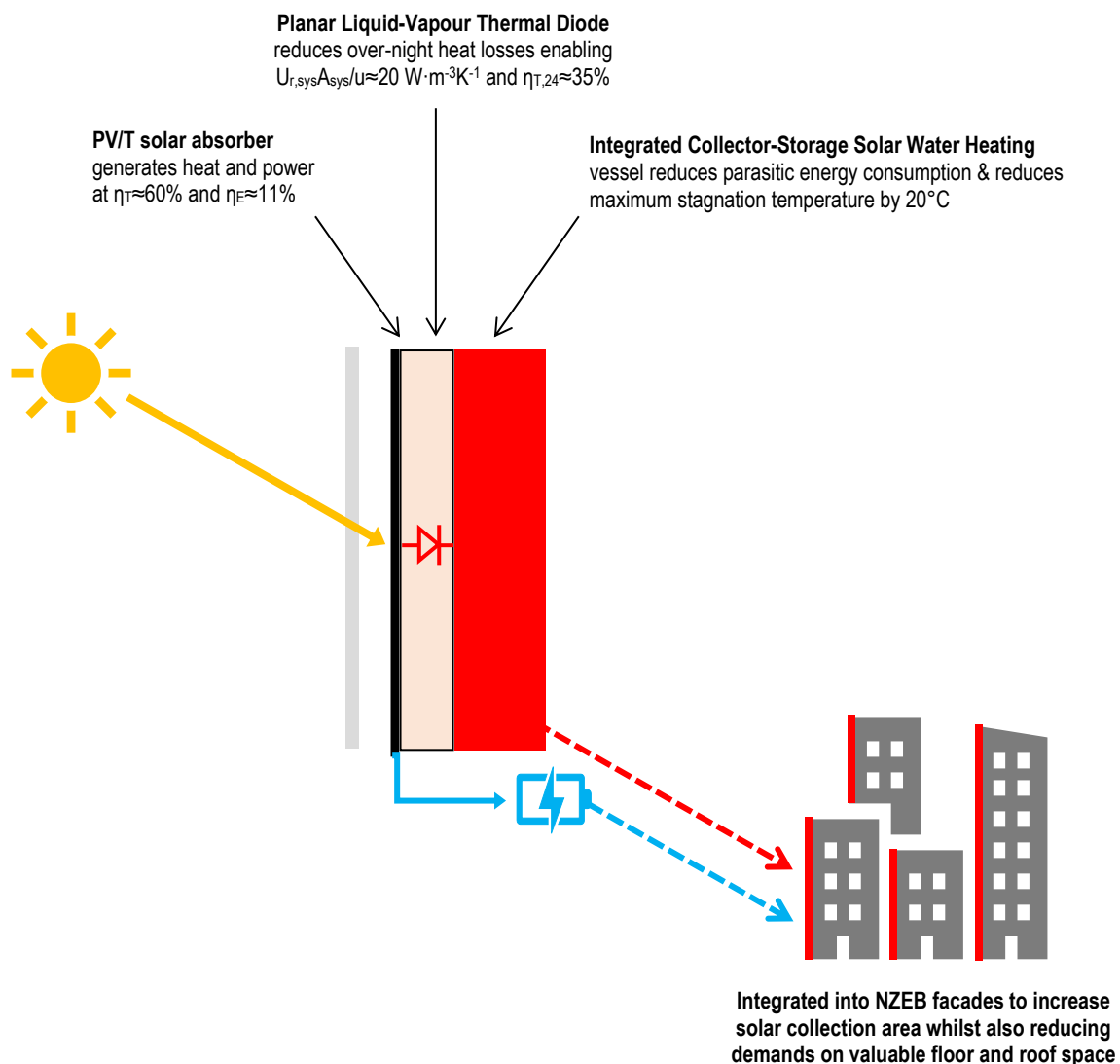
- Two-part study proposing an alternative approach to realising BIPV/T facades
- Part 1 reviews theory & potential, Part 2 describes prototype realisation & testing
- Integrated Collector-Storage Solar Water Heater element reduces overheating
- Planar Liquid-Vapour Thermal Diode element reduces overnight heat losses
- Model results show that approach meets conventional performance benchmarks

19 **Abstract**

20 Building Integrated Photovoltaic Thermal (BIPV/T) systems are promising solutions
21 for serving local electricity and heat demands in Net Zero Energy Buildings (NZEB).
22 Despite BIPV/T offering clear energetic and space saving advantages compared to
23 separate BIPV and solar thermal, overheating occurs when no thermal demand exists,
24 resulting in reduced yields, stagnation damage, and excessive fluid pressures. Whilst
25 continuous fluid flows mitigate overheating, corresponding parasitic demands and
26 space requirements are significant (pumps, large storage tanks or heat rejection
27 equipment). This two-part study examines an alternative approach to BIPV/T,
28 addressing overheating by combining BIPV and Integrated Collector-Storage Solar
29 Water Heater (ICSSWH) concepts. Solar heating capabilities of ICSSWH collectors
30 are well established and their overnight heat loss characteristics provide passive

31 overheating control. BIPV-ICSSWH approaches have yet to be investigated
 32 extensively. This paper (Part 1 of 2) reviews state-of-the-art and performance
 33 benchmarks in BIPV/T and ICSSWH; proposes new performance metrics enabling
 34 fairer comparisons; and develops a heat transfer model for BIPV-ICSSWH façade
 35 elements employing Planar Liquid-Vapour Thermal Diodes (PLVTD) to regulate
 36 absorber temperatures and heat losses. Multi-day solar thermal collection,
 37 photovoltaic generation, and overnight heat retention behaviours are simulated in
 38 different climates. The modelling results (experimentally validated in Part 2 of 2)
 39 suggests BIPV-PLVTD-ICSSWHs with single transparent covers and $\zeta \approx 90\%$ PLVTD
 40 diodicity achieve $\eta_{T,col} \approx 60\%$ solar thermal efficiency at $N \approx 0.035 \text{m}^2 \text{K} \cdot \text{W}^{-1}$, PV/T
 41 performance ratio $PR_{T3} \approx 75\%$, and heat loss coefficient $U_{r,sys} A_{sys} / u \approx 20 \text{W} \cdot \text{m}^{-3} \text{K}^{-1}$. The
 42 novel BIPV-PLVTD-ICSSWH approach can reduce maximum stagnation by 20°C
 43 compared to conventional BIPV/T and therefore support NZEB realisation during
 44 global efforts to tackle the climate crisis.

45 **Graphical abstract**



47 **1 Introduction**

48 Net-Zero Energy Buildings (NZEB) are increasingly being designed with Building
49 Integrated Photovoltaics (BIPV) to generate electricity and Building Integrated Solar
50 Thermal Systems (BISTS) to supply domestic hot water and thermal energy to
51 contribute towards space heating demands (COST, 2015). Approximately one-third of
52 global final energy consumption (125 of 400EJ annually) can be attributed to
53 residential and service sector buildings (IEA, 2018; IEA/UN, 2018) where it is primarily
54 used for space heating & cooling (40%) and domestic hot water production (20%).
55 Buildings are correspondingly responsible for ~39% of global CO₂ emissions which
56 need to be radically and rapidly cut in order to mitigate the climate crisis. For
57 residential and commercial buildings in a variety of climates, BISTS can provide
58 between 10% and 90% of space heating and domestic hot water energy demands
59 (Smyth et al., 2006; Li et al., 2013; Drosou et al., 2014; O'Hegarty et al., 2014; Good
60 et al., 2015; Mehdaoui et al., 2019; Beausoleil-Morrison et al., 2019; Billardo et al.,
61 2019) and BIPV can cover similarly large proportions of building electrical loads (Good
62 et al., 2015; Sorgato et al. 2018; Belussi, 2019; Li et al., 2019). Mismatches between
63 energy demands and solar availability (instantaneously, diurnally and over inter-
64 seasonal timescales) mean that thermal energy storage is an essential part of most
65 BISTS and is crucial for achievement of a high solar fraction. Electrical energy storage
66 is likewise crucial for high solar fraction BIPV systems and can be implemented in the
67 form of batteries or as "virtual storage" via an import-export connection to the grid,
68 perhaps in combination with load scheduling (Kats and Seal, 2012). Integrated
69 Collector-Storage Solar Water Heater (ICSSWH) concepts have potential to reduce the
70 costs of BISTS and to minimise loss of valuable floor space associated with
71 conventional solar hot water storage. Very few authors (Krauter, 2004; Ziapour et al.,
72 2014; Pugsley et al., 2016) have considered the potential for combining PV and
73 ICSSWH concepts, integrating ICSSWHs into building facades (Smyth et al., 2019;
74 Harmim et al., 2019), or using them as a thermal source for heat pumps (Pugsley et
75 al., 2017). The present work examines the synergy of combining PV and ICSSWH
76 concepts in the BIPV and BISTS context and explores potential benefits of introducing
77 Planar Liquid-Vapour Thermal Diodes (PLVTDs) to improve PV-thermal heat transfer
78 and reduce overnight heat losses.

79 Traditionally, solar thermal and photovoltaic collectors have been applied as bolt-on
80 elements to building envelopes, usually fixed to roofs and tilted towards the equator
81 at the latitude angle to maximise annual insolation, or in some cases fixed to facades.
82 These building applied collectors compete for available space and can adversely affect
83 the visual aesthetics of building exteriors. Table 1 summarises insolation and average

84 irradiance levels for three contrasting climate locations (Belfast, UK; Rome, Italy;
85 Riyadh, Saudi Arabia) at different latitudes based on 22 years of extra-terrestrial solar
86 radiation measurements and earth surface satellite imagery (NASA, 2019; Stackhouse
87 et al., 2018). Large seasonal and locational variations are apparent for horizontal
88 ($100 < G_{avg} < 600 \text{ W/m}^2$ and $3 < H_{24} < 27 \text{ MJ/m}^2$), latitude tilted ($200 < G_{avg} < 600 \text{ W/m}^2$ and
89 $5 < H_{24} < 24 \text{ MJ/m}^2$) and sun tracking surfaces ($200 < G < 800 \text{ W/m}^2$ and $6 < H_{24} < 37$
90 MJ/m^2). Equator-facing vertical surfaces consistently receive $200 < G_{avg} < 500 \text{ W/m}^2$ and
91 $4 < H_{24} < 14 \text{ MJ/m}^2$ for all three locations which represents a much more seasonally
92 stable resource, albeit of generally lower intensity. The daily insolation received by a
93 vertically oriented equator-facing surface corresponds to 60-75% of the maximum
94 available (relative to a sun-tracking surface) in winter and 19-46% of the maximum
95 available energy in summer. It should be noted that much higher instantaneous
96 irradiances ($G_{inst} \approx 1000 \text{ W/m}^2$, occasionally higher due to cloud reflections) will occur
97 on clear sunny days at times when the sun is aligned normal to the collector plane.

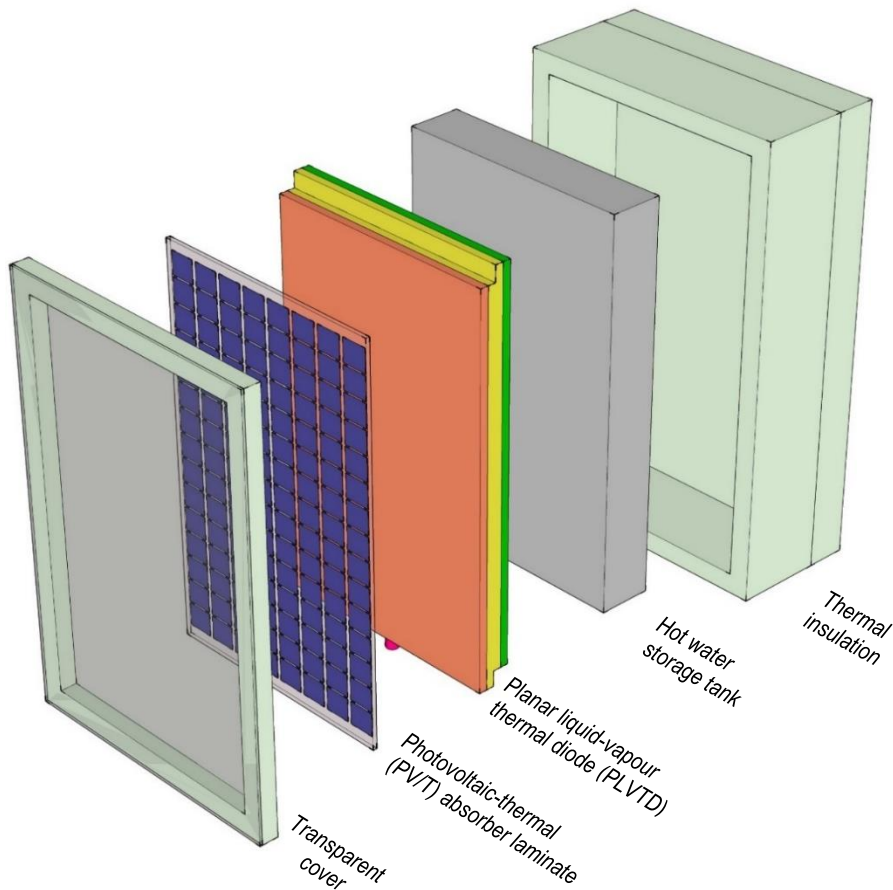
98 Building Integrated Photovoltaic-Thermal (BIPV/T) systems combine solar electricity
99 and thermal energy (hot air and/or water) generation into the building envelope. The
100 collectors form an integral part of the architecture to make aesthetically pleasing and
101 efficient use of all available insolated building envelope surfaces. This becomes
102 increasingly important for NZEBs, especially where there is a high ratio of energy
103 demand to envelope surface area, and in particular to the case of relatively tall
104 buildings (Saretta et al., 2020) where roof space for solar collectors (and likewise land
105 area for ground source heat collection) is inherently limited. Façade integrated BIPV/T
106 is a good option in higher latitude locations (such as Belfast) where significant energy
107 is required for heating and lighting in winter when the solar altitude is low and vertical
108 surfaces receive more insolation than horizontal surfaces (see Table 1). Despite
109 offering clear energetic advantages when suitable thermal demands exist, PV/T
110 collectors suffer similar stagnation and overheating problems as closed-back BIPV
111 systems (ie reduced electrical yields and eventual delamination damage) and
112 conventional solar flat plate solar water heaters (ie over-pressurisation, denaturing of
113 heat transfer fluids, damage to selective coatings, melting of polymeric components)
114 when no thermal demands exist. This can be avoided by ensuring continuous fluid
115 flows on hot sunny days but the corresponding parasitic energy requirements (eg for
116 pumps and/or heat rejection fans) typically far exceed the modest gains in electrical
117 yields and the ancillary equipment (large thermal stores and/or heat rejectors) occupy
118 valuable floor space.

Table 1 – Comparison of solar radiation levels on horizontal, vertical, tilted, and sun-tracking surfaces at different latitudes

Location (Latitude, Longitude)		Cool, wet and cloudy climate	Warm and sunny climate	Hot, dry and very sunny climate
		Belfast, UK (54.6N, 5.9W)	Rome, Italy (41.9N, 12.5E)	Riyadh, Saudi Arabia (24.6N, 46.7E)
Annual global horizontal insolation ^(a) (H_{h365} , MJ/m ²)		3247	6073	7495
Summertime ^(a) average daily insolation (H_{24} , MJ/m ²)	Horizontal surface	15.3	25.8	26.6
	Sun tracking surface	20.4	37.3	35.8
	Latitude tilted surface	13.8	23.8	24.3
	Vertical surface	9.4	11.5	6.9
	Daylight hours duration (t_{day} , hours)	16.2	14.6	13.4
Wintertime ^(a) average daily insolation (H_{24} , MJ/m ²)	Horizontal surface	2.7	7.7	14.2
	Sun tracking surface	5.9	16.8	23.7
	Latitude tilted surface	4.7	13.1	17.6
	Vertical surface	4.4	12.4	14.3
	Daylight hours duration (t_{day} , hours)	8.4	9.8	10.9
Summertime ^(b) typical irradiance (G_{avg} , W/m ²)	Horizontal surface ^(c)	279	527	596
	Sun tracking surface ^(c)	373	762	802
	Latitude tilted surface ^(d)	270	525	592
	Vertical surface ^(e)	215	292	191
Wintertime ^(b) typical irradiance (G_{avg} , W/m ²)	Horizontal surface ^(c)	101	243	398
	Sun tracking surface ^(c)	221	530	665
	Latitude tilted surface ^(d)	204	467	549
	Vertical surface ^(e)	194	469	486

Table notes:

- Data from NASA (2019) based on averages for the summer months May, June, July and August and winter months November, December, January and February. Values for sun tracking collectors are based on total diffuse plus direct radiation.
- Based on average daily insolation level divided by the estimated number of "useful" daylight hours.
- The number of "useful" daylight hours for a sun tracking surface is taken to be 1 hour less than the total number of daylight hours to account for the fact that the sun is partially obscured by the horizon at dawn and dusk.
- The number of "useful" daylight hours for horizontal and equator-facing latitude-tilted surfaces is taken as 2 hours less than the total number of daylight hours. This is to reflect the fact that the sun is incident at grazing angles (<15° relative to the collector plane) during the first and last hours of the day, which results in these surfaces receiving <25% of the available direct beam irradiance.
- The number of "useful" daylight hours for equator-facing vertical surfaces is taken as 75% of the total number of daylight hours to account for dawn and dusk grazing incidence angles (as explained in Note "d") plus additional grazing incidence angles which occur near solar noon at low latitude locations during summer.



135
 136 **Figure 1: Key components of the BIPV-PLVTD-ICSSWH concept**

137
 138 Integrated Collector-Storage Solar Water Heaters (ICSSWH) are an alternative to
 139 conventional flat plate or evacuated tube collector solar water heating systems. Whilst
 140 ICSSWH systems suffer significant overnight heat losses (eg unavailability of stored
 141 heat for morning bathing etc) they offer a number of advantages in respect of cost,
 142 space, and inherent passive protection from overheating. Development of the novel
 143 BIPV-PLVTD-ICSSWH concept proposed in this two-part study has the potential to
 144 overcome key problems associated with the individual technologies (namely, BIPV/T
 145 overheating during stagnation, and ICSSWH overnight heat losses) and to realise new
 146 synergies. An exploded diagram illustrating the component parts of a BIPV-PLVTD-
 147 ICSSWH collector is shown in Figure 1. The present paper (Part 1 of 2) introduces the
 148 BIPV-PLVTD-ICSSWH concept; reviews the fundamental operating principles of PV/T,
 149 ICSSWH and PLVTD components; and establishes state-of-the-art performance
 150 benchmarks. A new heat loss performance metric ($U_{r,sys}A_{sys}/u$ with units $W \cdot m^{-3} \cdot K^{-1}$) is
 151 proposed to enable ICSSWHs of differing sizes and shapes to be compared more fairly.
 152 New thermal and electrical performance metrics (diurnal thermal efficiency $\eta_{T,24}$ and
 153 PV/T performance ratio PR_{T3}) are also proposed to facilitate better comparisons

154 between different technologies. An energetic model of the BIPV-PLVTD-ICSSWH
155 concept is presented and some key theoretical considerations concerning heat removal
156 factors and thermal diodicity are discussed. The energy model has been used to predict
157 temperatures, solar thermal collection, photovoltaic generation, and overnight heat
158 retention behaviours over multi-day periods in a variety of climates. Modelling results
159 have been compared with appropriate benchmarks to highlight the potential benefits
160 of the BIPV-PLVTD-ICSSWH concept in the context of applications in NZEB facades.
161 The concluding part of the study is presented in a separate paper (Part 2 of 2) which
162 describes realisation and laboratory testing of a prototype to demonstrate operation
163 and validate the theoretical model.

164

165 **2 State-of-the-art in relevant technologies**

166 **2.1 Photovoltaic-thermal (PV/T) systems**

167 The concept of combining PV and thermal absorbers into a single collector initially
168 arose from a need to remove unwanted heat from early PV modules (especially those
169 incorporating concentrating reflectors) whose electrical efficiency was compromised by
170 high temperatures. The first PV/T collectors were designed to use this “waste” heat for
171 residential water and air heating applications. Zondag (2008) gives a comprehensive
172 review of 30 years of flat plate PV/T collector development and more recent reviews
173 are given by Michael et al. (2015); Besheer et al. (2016) and Sultan & Efzan (2018),
174 amongst others. Whilst popularity of PV systems has sky-rocketed in recent years
175 owing to rapidly declining costs, PV/T systems have failed to achieve commercial
176 success. Recent academic advances in PV/T collector development have explored the
177 use of nanofluids to improve heat transfer and nanomaterials for phase change thermal
178 storage or optical filtering (Abdelrazik et al., 2018; Das et al., 2018). Recent advances
179 in system-level approaches, applications, and economics of BIPV/T (Buonomano et al.,
180 2016; Yang & Athienitis, 2016; Barone et al., 2019) include studies on heat pump
181 integration (Good et al., 2015; Calise et al., 2016; Qu et al., 2016) and the
182 multifunction façade context (Li et al., 2019; Tian et al., 2019).

183 **2.2 Electrical behaviour of PV/T systems**

184 Electrical efficiencies of PV/T collectors are typically 5 to 15% depending on PV cell
185 material type and heat delivery temperature. The main drivers of electrical efficiency
186 (assuming no shading) are the inherent PV cell efficiency characteristics; cell operating
187 temperature; and optical losses. Individual PV cells each nominally produce ~0.5V,

188 although voltage reduces with increasing temperature and tends towards zero under
189 low irradiance or short circuit conditions. Current flows depend upon PV cell material
190 type and are proportional to area and incident irradiance level; inversely proportional
191 to applied electrical load resistance (tending to zero under open circuit conditions);
192 and typically increase slightly with increasing cell temperature. Cells connected
193 together in series all operate at the same current, while cells connected in parallel all
194 operate at the same voltage. Temperature gradients sometimes exist over PV/T
195 absorber surfaces causing cells to operate at different maximum power points.
196 Operating point voltage differences caused by temperature non-uniformities can
197 significantly reduce electrical efficiency if cells are connected in parallel but generally
198 have minimal effect on series connected cells. Monocrystalline (mc-si) and
199 polycrystalline (pc-si) silicon PV cells, and amorphous silicon (a-si), Cadmium Telluride
200 (CdTe) and Copper Indium Gallium Selenide (CIGS) thin film cells have all successfully
201 been used for PV/T. Crystalline silicon typically offers high efficiency ($15 < \eta_E < 18\%$) at
202 low temperatures but pronounced reductions occur with increasing temperature. Lower
203 efficiencies ($6 < \eta_E < 12\%$) are typical for thin film cell types. Multijunction cells, formed
204 of several layers of different PV materials with different band gaps, have the highest
205 known photovoltaic efficiencies but are expensive and typically only used for spacecraft
206 applications. Inclusion of transparent covers over PV/T absorbers significantly reduces
207 heat loss but correspondingly increases optical losses and hence reduces electrical
208 efficiency. Experimental work by Guarracino et al. (2019) found that transparent
209 covers can significantly reduce electrical efficiency, especially at oblique solar incidence
210 angles when reflection losses are typically more significant than cell temperature
211 effects. Zondag (2008) suggests uncovered BIPV/T façade electrical efficiencies are
212 commonly enhanced by $\sim 10\%$ compared to non-ventilated BIPV due to beneficial heat
213 removal but can be compromised by $\sim 10\%$ compared to conventional naturally
214 ventilated roof-mounted PV modules if heat delivery temperatures are high (similar
215 findings are reported by Fuentes et al., 2018). Net electrical yields from BIPV/T
216 systems can be lower than those from BIPV owing to the parasitic electricity
217 consumption by pumps and fans facilitating heat removal. Parasitic consumption
218 increases when buildings have no significant heat demand (eg no space heating
219 required in summer and relatively low hot water usage) and waste heat rejection
220 equipment becomes necessary to prevent overheating damage caused by stagnation
221 (delamination, excess fluid pressures, etc).

222 Cells and modules are commonly characterized with reference to Standard Test
223 Conditions (STC at $G=1000 \text{ W/m}^2$ irradiance with spectrum AM1.5 and $T_0=25^\circ\text{C}$ cell

224 temperature) using performance metrics derived from current-voltage curves. Key
225 metrics (defined in Equations 1 to 4) include short circuit current (I_{sc}), open circuit
226 voltage (V_{oc}), electrical power delivered at the maximum power point ($q_{E,mp}$), fill factor
227 (FF), voltage-temperature coefficient ($K_{V:T}$), current-temperature coefficient ($K_{I:T}$) and
228 voltage-irradiance coefficient $K_{V:G}$. Performance deviates from the ideal current-voltage
229 curve ($FF_{ideal} = 1$) with increasing irradiance and increasing temperature such that
230 typical real values are $0.75 < FF_{STC} < 0.85$ and $K_{V:T} = -0.45\%/K$ for c-si and
231 $0.5 < FF_{STC} < 0.7$ and $K_{V:T} = -0.25\%/K$ for thin film (DGS, 2008). Current-temperature
232 coefficients ($K_{I:T}$) and are usually positive but an order of magnitude smaller than $K_{V:T}$.
233 According to Santbergen et al. (2010) non-linear voltage-irradiance coefficient values
234 are typically $K_{V:G} \approx 100\%$ for irradiances of primary interest ($400 < G < 1200 \text{ W}\cdot\text{m}^{-2}$),
235 $K_{V:G} \approx 80\%$ for cloudy conditions ($G = 100 \text{ W}\cdot\text{m}^{-2}$) and $K_{V:G} < 50\%$ for very low irradiances
236 ($G < 50 \text{ W}\cdot\text{m}^{-2}$).

237 The electrical output of a conventional PV module operating under realistic conditions
238 deviates significantly from that occurring under STC owing to a variety of cell
239 temperature and irradiance effects. Cell temperatures (T_0) are determined by the
240 ambient temperature (T_a) and incident irradiance level (G) as well as module mounting
241 arrangements and local wind speed effects. Irradiance incident on the PV cell surface
242 is determined by the prevailing irradiance level and spectrum (which are functions of
243 latitude, time of day, module mounting angle, and local weather conditions) as well as
244 optical losses associated with cell coverings (eg cover glass, cell encapsulation
245 materials, front-of-cell electrical contacts etc). Deviations relative to STC are further
246 pronounced in the case of PV/T modules owing to the influence of the fluid temperature
247 (T_3) upon the cell temperature (T_0) and because transparent covers required to reduce
248 heat loss inherently reduce the effective transmissivity (τ). A sensible approach to the
249 characterization of PV/T module electrical performance is therefore to define a
250 Performance Ratio comparing the device's maximum electrical power output (q_{E,mp,T_3})
251 at operating fluid temperature (T_3) relative to a chosen reference value. Santbergen
252 et al. (2010) use the standard maximum power output (q_{STC}) as the reference value
253 (PR_{STC} as defined by Equation 5). We propose an alternative (PR_{T_3} as defined by
254 Equation 6) which takes the reference value as being the power output of an ideal PV/T
255 module with perfect optical ($\tau = 1$) and heat transfer characteristics ($F = 1$ so that $T_0 = T_3$)
256 and full coverage of the absorber by PV cells ($A_0 = A_1$). Based on work of other authors
257 (notably Zondag et al., 2003; Santbergen et al., 2010 and Guarracino et al., 2019)
258 suitable benchmark values are $PR_{T_3} = 85\%$ and $PR_{T_3} = 75\%$ for uncovered and covered
259 collectors respectively.

$$260 \quad q_{E,mp} = I_{mp} \cdot V_{mp} = FF \cdot I_{sc} \cdot V_{oc} \quad \text{Equation 1}$$

$$261 \quad K_{V:T} = \frac{V_{oc,T_0} - V_{oc,STC}}{V_{oc,STC} (T_0 - 25)} \quad \text{Equation 2}$$

$$262 \quad K_{I:T} = \frac{I_{sc,T_0} - I_{sc,STC}}{I_{sc,STC} (T_0 - 25)} \quad \text{Equation 3}$$

$$263 \quad K_{V:G} = \frac{V_{oc,G}}{V_{oc,STC}} \quad \text{Equation 4}$$

$$264 \quad PR_{STC} = \frac{\text{Electrical efficiency of PVT operating at } T_3}{\text{Electrical efficiency of single cell operating at STC}} = \frac{\eta_{E,mp,T_3}}{\eta_{STC}} = \frac{q_{E,mp,T_3} (G \cdot A_1)^{-1}}{q_{STC} (G_{STC} \cdot A_0)^{-1}} \quad \text{Equation 5}$$

$$265 \quad PR_{T_3} = \frac{\text{Electrical efficiency of PVT operating at } T_3}{\text{Electrical efficiency of single cell operating at } T_3} = \frac{PR_{STC}}{2 - (1 - [T_3 - 25]K_{V:T}) \cdot (1 - [T_3 - 25]K_{I:T})} \quad \text{Equation 6}$$

266 **2.3 Thermal behaviour of PV/T systems**

267 Solar thermal efficiencies of PV/T collectors are typically $60 < \eta_T < 80\%$ when working
 268 fluid and ambient temperatures are equal (zero loss condition) but commonly $\eta_T < 30\%$
 269 for collectors producing domestic hot water in cool climates. Cell type and packing
 270 factor; front-of-cell electrical contacts or transparent conductors; absorber substrate
 271 characteristics; and encapsulation material properties, together determine the optical
 272 properties and heat transfer characteristics of PV/T absorbers. Solar thermal efficiencies
 273 of PV/T absorbers are generally lower than those of dedicated solar heat collectors
 274 because absorption coefficients ($0.7 < \alpha < 0.9$) and emissivities ($0.2 < \varepsilon < 0.6$ bare or
 275 $0.7 < \varepsilon < 0.9$ encapsulated) of PV cells are inferior to those achieved by solar selective
 276 coatings ($\alpha \approx 0.95$ and $\varepsilon \approx 0.1$). Thermal efficiencies are also inherently reduced because a
 277 proportion of the input solar energy is converted to electricity when a suitable load is
 278 connected (Guarracino et al., 2019). High emissivities of PV cells and encapsulation
 279 materials increases radiative heat losses which become particularly significant at high
 280 heat delivery temperatures. Typical PV/T collector constructions are discussed in detail
 281 by Santbergen et al. (2010) and Dupeyrat et al. (2011). Most liquid-heating PV/T
 282 collectors take the form of individual PV cells or whole module laminates glued or bonded
 283 to conventional metal solar thermal absorbers (eg sheet-and-tube, flow channel, or roll-
 284 bond types). High thermal conductance through bonding layers joining PV cells to
 285 absorber substrates is required to minimise absorber temperatures, minimise heat
 286 losses, and maximise solar thermal efficiency. Likewise, convective heat transfer
 287 between absorber substrates and working fluids should be maximized. Zondag (2008)
 288 discusses PV/T collectors featuring overall conductances in the range 40 to

289 250 W·m⁻²K⁻¹ with the poorest example of heat transfer occurring in a collector
290 featuring a 5mm silicone bonding layer where cell-to-fluid temperature difference was
291 12°C corresponding to >10% reduction in thermal output and ~5% reduction in
292 electrical yield. Dupeyrat et al. (2011) fabricated a high efficiency collector with 0.5mm
293 thick Ethylene-Vinyl Acetate bonding layer achieving 700 W·m⁻²K⁻¹ between PV cells and
294 a 1.2mm roll-bond aluminium thermal absorber. Fragile PV cells must be protected
295 against damaging mechanical forces (eg torsions during handling, wind loads, and
296 impacts from hail or vandalism); protected against water ingress; and electrically
297 isolated from metal substrates. External protection usually takes the form of a glass
298 or transparent polymer layer bonded to the front side of the PV cells. This can be
299 supplemented by one or more tertiary transparent covers to reduce heat loss in cases
300 where high delivery temperatures or operation in cold and windy climates is required
301 (ie heat delivered at >20°C higher than ambient). Like conventional solar thermal
302 collectors, PV/T must be protected against high stagnation temperatures (especially
303 when fitted with tertiary transparent covers) and withstand thermal shocks caused by
304 rapid changes in climatic conditions or fluid flow transients (eg cold water flowing into
305 hot collectors). Damage can occur due to high fluid pressures; differential thermal
306 expansion stresses; melting and UV light degradation of polymeric component
307 materials. Stagnation damage prevention requires continuous operation of fluid
308 circulation systems during hot and sunny periods and heat rejection systems may be
309 required when thermal demands are low or intermittent.

310 **2.4 Integrated Collector-Storage Solar Water Heaters**

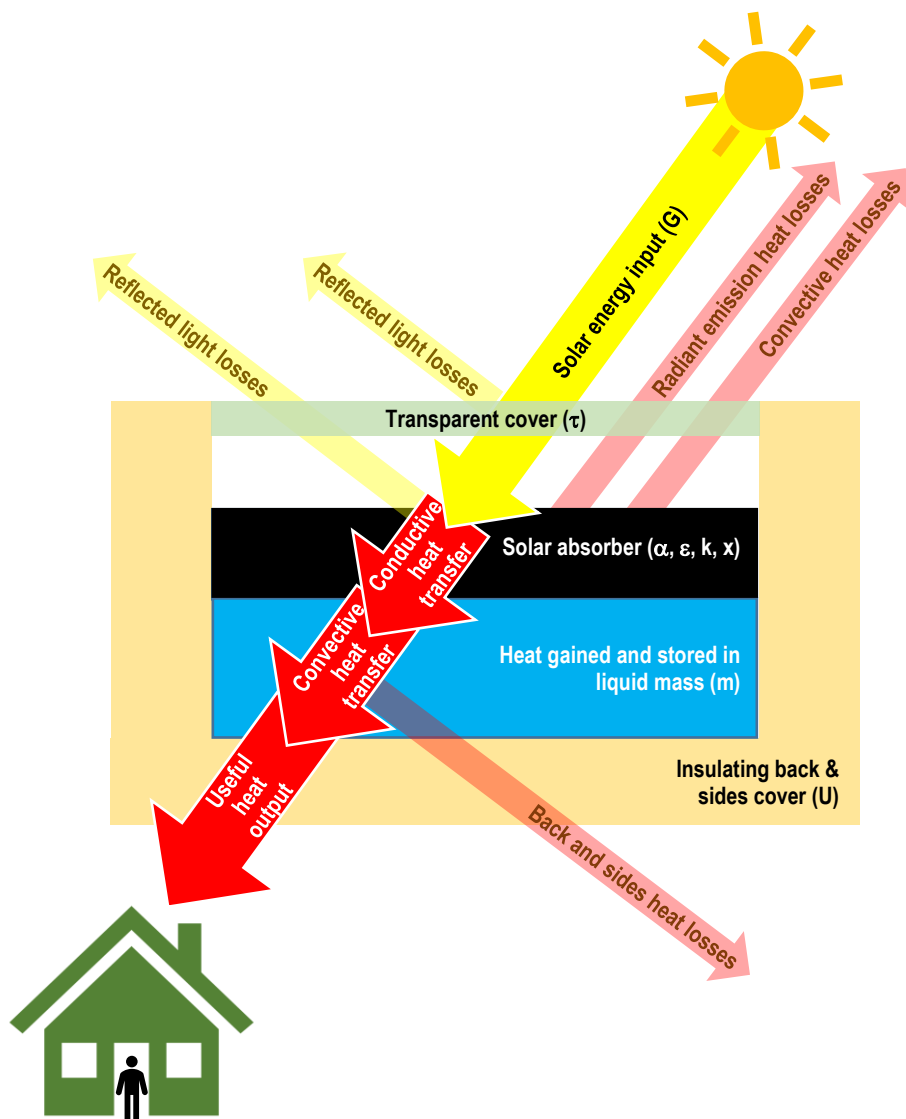
311 Solar water heating systems typically have three main components: the collector, the
312 heat transfer system, and the storage vessel. Storage vessels in conventional pumped
313 solar water heating systems tend to be bulky and consume valuable floor space. In hot
314 climates, thermosiphon solar water heaters with close-coupled storage tanks are
315 popular owing to their passive operation, simple installation, externally located storage
316 tank, and relatively low cost. Integrated Collector-Storage Solar Water Heaters
317 (ICSSWH) combine the solar absorber and the thermal storage tank into a single unit
318 to save floor space within the building and to reduce the amount of pumping energy
319 required. They are usually passive devices in which part of the storage tank envelope
320 is used as a solar absorber. This minimises system size and quantity of material
321 required for manufacturing, leading to lower unit costs (Tripanagnostopoulos &
322 Souliotis, 2006), less embodied energy, and greater space efficiency. The greatest
323 drawback of ICSSWHs and close-coupled thermosiphon solar water heaters is that a

324 large area of storage vessel surface is inherently exposed to the outdoor environment
325 and thus susceptible to heat loss, especially in cold and windy climates. Smyth et al.
326 (2006) provides a comprehensive review from a technical perspective and traces
327 development history back to the 1800s. A more recent review by Singh et al. (2016)
328 attempts to categorise designs according to whether they are non-concentrating (eg
329 flat plate or tank box systems), concentrating (eg compound parabolic) or employing
330 phase change materials. The working principle of an ICSSWH is shown in Figure 2 and
331 the key components and design considerations are:

- 332 • **Collector inclination and orientation** affects diurnal and seasonal variation
333 of solar radiation incident on absorber surfaces and also affects natural
334 convection and storage tank stratification.
- 335 • **Transparent covers** minimize convective (and some radiative) absorber heat
336 losses and are essential for ICSSWH collectors designed to produce domestic
337 hot water or to operate in cold and windy climates.
- 338 • **Storage tank size, shape, & configuration** affect collection and retention
339 efficiencies, stratification and achievable temperature. Tanks are usually heavily
340 insulated on their non-absorbing sides to reduce heat loss.
- 341 • **Fabrication material choices** are the primary factor determining cost but also
342 affect solar absorption and heat transfer characteristics (desired solar gains and
343 unwanted losses), robustness and longevity.

344 Original academic works on ICSSWH technologies over the last decade have examined
345 tank temperature stratification and draw-off mixing effects (Garnier et al., 2009;
346 Borello et al., 2012); use of thermal diodes and concentrating reflectors to reduce heat
347 loss (Souliotis et al., 2011&2017; Smyth et al., 2015a&b, 2017, 2018, 2019;
348 Muhumuza et al., 2019a&b and 2020); and use of phase-change thermal storage
349 materials and heat pipes (Tarhan et al., 2006; Eames & Griffiths, 2006; Chaabane,
350 2014; Bilardo et al., 2019). Studies by Krauter (2004) and Ziapour et al. (2014)
351 examined the performance (respectively through experimental and simulation work)
352 of novel PV-ICSSWH devices and identified a dearth of published work on similar
353 concepts. Facade integration of PV-ICSSWH units (Pugsley et al., 2016 & 2017; Smyth
354 et al., 2019) has potential to increase available solar collection area, save floor space,
355 reduce parasitic pumping energy requirements, and reduce material costs, but
356 presents a number of practical challenges such as imposed structural loadings and
357 maintenance access arrangements (considered in more detail in Part 2 of 2).

358



359

360 *Figure 2: Energy conversion and loss mechanisms in ICSSWH*

361

362 Almost all ICSSWH collectors feature some form of transparent cover because
 363 overnight tank heat losses from uncovered absorbers would result in unacceptably low
 364 morning-time tank temperatures. Solutions such as double covers, thermal diodes, or
 365 heat pipes need to be considered for ICSSWH systems designed to produce domestic
 366 hot water when operating in cold and windy climates. The volume-to-absorber area
 367 ratio (v/A) is an important consideration in ICSSWH design as this determines the rate
 368 at which the tank gains heat from the incident sunlight during collection periods and
 369 also the rate at which heat is lost from the absorber to the ambient environment during
 370 retention periods (cloudy or overnight). Storage tank shape can significantly affect the
 371 solar collection and heat retention performances (owing to its influence on absorber
 372 orientation and exposure; thermal stratification; and overall heat loss coefficients) as
 373 well as physical robustness and aesthetics. In particular, tall tanks tend to promote
 374 stratification (which maximises potential heat delivery temperatures); triangular and

375 trapezoidal shapes enable inherent tilting of absorber surfaces (to align with the sun);
376 whilst cylindrical tanks offer inherent passive single-axis solar tracking and tend to be
377 more robust than cubic tanks. Tank envelopes must support the weight of water
378 contained within them and be able to withstand thermal expansion pressures (sealed
379 units/systems) and any externally imposed hydraulic pressures (from mains water or
380 raised header feed tanks). Tanks must be insulated to minimise heat loss from the
381 back and sides (those not used to absorb solar heat) but the insulation thickness can
382 add significantly to overall size. Smyth et al. (2006) and Singh et al. (2016) cite
383 numerous ICSSWH collector examples featuring single or multiple cylindrical, cuboid,
384 triangular, trapezoidal and pyramid tanks with volume-to-absorber area ratios in the
385 range $0.05 < u/A < 0.3 \text{ m}^3/\text{m}^2$ with $0.1 \text{ m}^3/\text{m}^2$ being a typical tank size. Small volumes
386 of stored water cause large diurnal temperature fluctuations in solar heating systems.
387 Larger volumes reduce fluctuation magnitudes thereby reducing summertime
388 overheating and wintertime freezing risks, but the resulting reduced maximum
389 temperatures can increase legionella risks. Schmidt & Goetzberger (1990) suggest
390 $u/A > 0.07 \text{ m}^3/\text{m}^2$ for Northern European climates to reduce freeze risks. Amerongen et
391 al. (2013) suggests limiting criteria of $u/A < 0.03 \text{ m}^3/\text{m}^2$ and $u/A < 0.06 \text{ m}^3/\text{m}^2$ for
392 northern and southern European climates respectively in respect of controlling
393 legionella risk in direct-flow solar water heating systems. Using ICSSWH principles in
394 the context of BIPV/T presents an opportunity to prevent damagingly high stagnation
395 temperatures without the need for heat rejection equipment and offers significant
396 potential benefits in terms of reducing parasitic energy consumption for fluid pumping.
397 Such systems should be designed as indirect-flow types which employ heat exchangers
398 to mitigate legionella risk.

399 **2.5 Solar thermal collection and heat retention behaviour**

400 The thermal power output (q_T) of solar thermal collectors is conventionally represented
401 in the Hottel-Whillier-Bliss form (Equation 7) and presented in the form of efficiency
402 curves (see Figure 3) where the x-axis is the solar thermal condition (N according to
403 Equation 8) and the y-axis is the instantaneous solar thermal collection efficiency (η_T
404 according to Equation 9). On such plots, the y-axis intercept indicates maximum solar
405 thermal efficiency under zero heat loss conditions ($\eta_T = F \cdot \tau \cdot \alpha$ where $T_3 - T_a = 0$); the line
406 gradient ($F \cdot U_L$) represents the overall heat loss coefficient referenced to the absorber
407 area (A_1); and the x-axis intercept indicates the stagnation condition (maximum
408 achievable temperature for a given N when $\eta_T \rightarrow 0$ and $T_3 = T_1$). The y-axis intercept is
409 sometimes referred to as the "optical efficiency" because many conventional solar
410 thermal collectors achieve near perfect absorber-to-fluid heat transfer under these
411 conditions ($F > 0.95$) and overall efficiency is determined by the transmission-

412 absorption product ($\tau \cdot \alpha$). Heat removal factor (F) describes the effectiveness of
 413 absorber-to-tank heat transfer which can be expressed according to Equation 10.
 414 Production of electricity reduces the amount of heat available for transfer into the tank
 415 thus Equation 10 remains valid for the hypothetical scenario of 100% electrical
 416 efficiency where $q_E = G \cdot A_1$ which would result in $F = 0$.

417
$$q_T = F \cdot G \cdot A_1 \left([\tau \cdot \alpha] - \left[U_L \frac{T_3 - T_a}{G} \right] \right)$$
 Equation 7

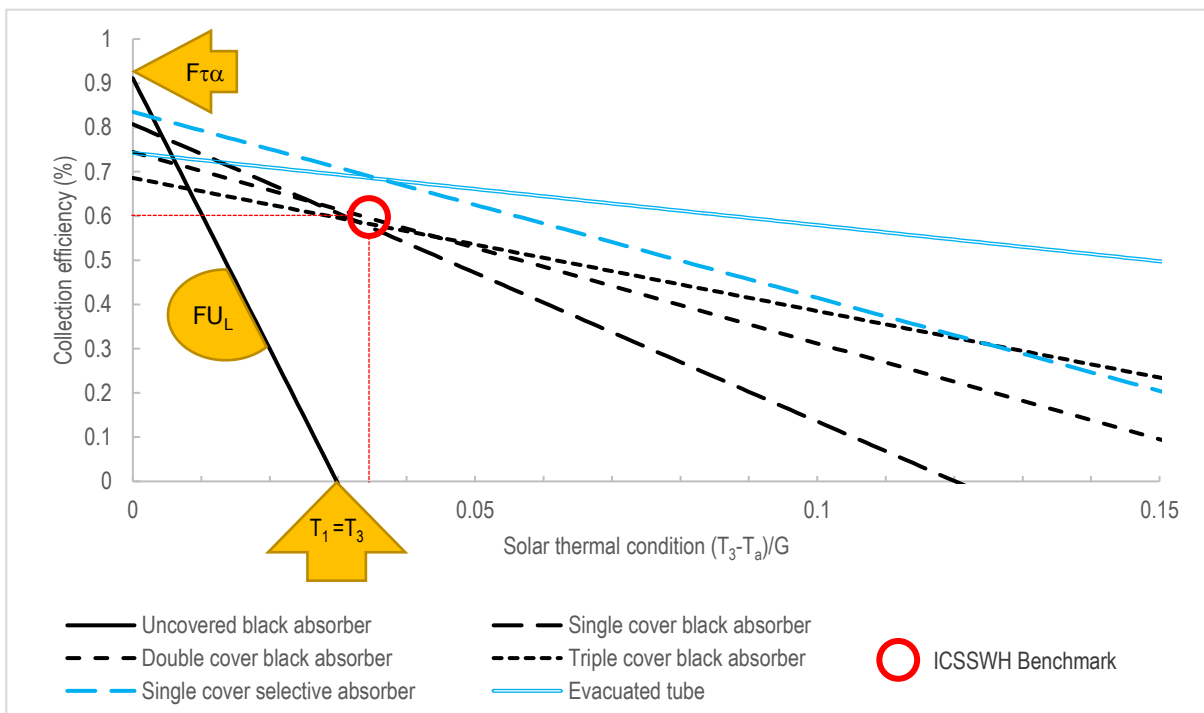
418
$$N = \frac{T_3 - T_a}{G}$$
 Equation 8

419
$$\eta_T = \frac{q_T}{G \cdot A_1}$$
 Equation 9

420
$$F = \frac{\text{Heat transferred}}{\text{Maximum heat available}} = \frac{q_T}{[\tau \cdot \alpha - \eta_E] \cdot G \cdot A_1}$$
 Equation 10

421
$$-q_T = U_{r,sys} A_{r,sys} (T_3 - T_a)$$
 Equation 11

422



423

424 **Figure 3: Typical solar collector performance characteristics (at 2m/s wind speed)**

425

426 Equations 7-10 are only relevant when the collector is illuminated ($G > 0$). When the
 427 ICSSWH is in darkness, the total heat loss ($-q_T$) is determined by the overall heat loss
 428 coefficient (U_{sys}) referenced to the overall envelope heat loss area (A_{sys}) and the
 429 temperature difference between the tank and the ambient ($T_3 - T_a$) as expressed by
 430 Equation 11. The key difference between the collection and retention heat loss

431 coefficients is that U_{sys} describes the total heat loss from the storage tank assuming
432 that it emanates from the whole envelope (A_{sys}) whereas U_L describes the total heat
433 loss from the storage tank assuming that it emanates from the absorber (A_1) which is
434 separated from the storage tank by heat removal factor F . The effective heat loss area
435 can be taken as approximately equal to the absorber area ($A_{sys} \approx A_1$) if the storage tank
436 and sides of the collector are highly insulated or approximately equal to the whole
437 envelope area ($A_{sys} \approx A_1 + A_{3i}$) if the insulation of the storage tank and sides has similar
438 performance characteristics as the transparent cover. It is difficult to determine a
439 sensible value for A_{sys} in other less definite cases.

440 In the case of conventional solar thermal collectors where heat is extracted and
441 delivered by a continuous fluid flow, the thermal power gain can be determined through
442 steady state testing based upon the mass flow rate, specific heat capacity, and inlet-
443 to-outlet temperature difference ($q_T = m \cdot c_p \cdot \Delta T_{out-in}$). However, in the case of ICSSWH
444 devices, there is commonly no fluid flow during solar collection periods and thus steady
445 state conditions rarely occur (except in the very unusual case where a concurrent heat
446 demand exactly matches solar heat collection). Instead, the thermal power gained by
447 an ICSSWH is usually determined using either quasi steady-state or whole-day testing
448 based upon the rate of temperature rise of the stored thermal mass ($q_T = M \cdot c_p \cdot \Delta T_3 / t_{col}$).
449 Equation 12 defines the total insolation (H_{col}) during the collection period (t_{col}) to enable
450 determination of daily average solar thermal efficiency ($\eta_{T,col}$) according to
451 Equation 13. The ability of an ICSSWH collector to retain stored heat for a period of
452 time (t_{ret}) when no solar resource is available (eg at night when $G \approx 0$) can be quantified
453 in terms of heat retention efficiency ($\eta_{T,ret}$ according to Equation 14) which is defined
454 as the ratio of thermal energy in the tank at the end of the retention period ($t = t_{col} + t_{ret}$)
455 divided by the thermal energy in the tank at the start of the retention period ($t = t_{col}$).
456 Collection periods are chosen to represent specific latitudinal and seasonal
457 circumstances but are commonly taken as 6, 8 or 12 hrs ($t_{col} = 21600, 28800$ or $43200s$)
458 with corresponding retention periods of 18, 16 or 12 hrs ($t_{ret} = 64800, 57600$ or
459 $43200s$). Energy contained in the tank at a given time ($Q_{T[t]}$) is determined by the
460 product of its heat capacity ($M \cdot c_p$) and temperature ($T_{3[t]}$) normalised to respective
461 ambient temperatures at the end of the preceding collection period ($T_{a[t_{col}]}$) and
462 averaged throughout the retention period ($\bar{T}_{a[t_{ret}]}$). Retention efficiency can be used to
463 determine an overall reverse mode heat transfer coefficient ($U_{r,sys} A_{sys}$ according to
464 Equations 15) which describes heat lost across the tank-to-ambient temperature
465 difference ($T_{3[t=t_{col}]} - \bar{T}_{a[t_{ret}]}$). A corresponding overall forward mode heat transfer

466 coefficient can be defined ($U_{f,sys}A_{sys}$, according to Equation 16) to describe heat loss
 467 across the tank-to-ambient temperature difference during collection periods ($T_{3[t=t_{col}]} -$
 468 $\tilde{T}_{a[t_{col}]}$). Dynamic modelling of heat loss during retention periods ($-\Delta Q_{T[t_{ret}]}$) and heat
 469 gained during collection periods ($\Delta Q_{T[t_{col}]}$) can be performed using Equations 17 and 18
 470 which are essentially the inverse forms of Equations 15 and 16.

$$471 \quad H_{col} = \int_{t=0}^{t=t_{col}} G \quad \text{Equation 12}$$

$$472 \quad \eta_{T,col} = \frac{\text{Energy in store at } t=t_{col}}{\text{Energy incident from } t=t_0 \text{ to } t=t_{col}} = \frac{M \cdot c_p (T_{3[t=t_{col}]} - T_{3[t=t_0]})}{H_{col} \cdot A_1} \quad \text{Equation 13}$$

$$473 \quad \eta_{T,ret} = \frac{\text{Retained energy in store at } t=t_{col}+t_{ret}}{\text{Energy in store at } t=t_{col}} = \frac{M \cdot c_p (T_{3[t=t_{col}+t_{ret}]} - \tilde{T}_{a[t_{ret}]})}{M \cdot c_p (T_{3[t=t_{col}]} - T_{a[t=t_{col}]})} \quad \text{Equation 14}$$

$$474 \quad U_{r,sys}A_{sys} = \frac{M \cdot c_p}{t_{ret}} \ln \left(\frac{1}{\eta_{T,ret}} \right) \quad \text{Equation 15}$$

$$475 \quad U_{f,sys}A_{sys} = \frac{M \cdot c_p}{t_{col}} \ln \left(\frac{1}{\eta_{T,col}} \right) = F \cdot U_L A_1 \quad \text{Equation 16}$$

$$476 \quad -\Delta Q_{T[t_{ret}]} = Q_{T[t=t_{col}]} \frac{T_{3[t=t_{col}]} - \tilde{T}_{a[t_{ret}]}}{T_{3[t=t_{col}]} - T_{a[t=t_{col}]}} \left(1 - \left[e^{\frac{U_{r,sys} A_{sys} t_{ret}}{M \cdot c_p}} \right]^{-1} \right) \quad \text{Equation 17}$$

$$477 \quad \Delta Q_{T[t_{col}]} = F \cdot A_1 \left(H_{col} \cdot \tau \cdot \alpha - t_{col} U_L (T_{3[t=t_0]} - T_{a[t=t_0]}) \right) \left[e^{\frac{F \cdot U_L A_1 t_{col}}{M \cdot c_p}} \right]^{-1} \quad \text{Equation 18}$$

478 Heat could feasibly be drawn from the ICSSWH to serve a variety of thermal load
 479 demands at different times of the day (eg morning or evening bathing, space heating
 480 at night, etc). If all available heat is consumed during a single short duration draw-off
 481 event occurring once every 24h, the maximum availability of stored heat ($Q_{T,24max}$,
 482 Equation 19) occurs when the tank temperature reaches its maximum (near the end
 483 of the collection period, usually just before dusk) and minimum availability of stored
 484 heat ($Q_{T,24min}$, Equation 20) coincides with the time when the lowest tank temperature
 485 occurs (near the end of the retention period, usually around dawn). Provided that t_{col}
 486 and t_{ret} cover a contiguous 24h period then the product of the collection and retention
 487 efficiencies can reasonably be described as the diurnal thermal efficiency, where
 488 $\eta_{T,24}=1$ if all available solar energy incident during t_{col} is collected and then retained
 489 without loss for the duration of t_{ret} , or $\eta_{T,24}=0$ if no heat was collected or all collected
 490 heat was lost. The total diurnal efficiency ($\eta_{T+E,24}$) is the sum of the diurnal thermal
 491 efficiency and the diurnal electrical efficiency ($\eta_{E,24}$) and can be defined according to

492 Equation 21. It is important to note that diurnal thermal efficiency (by this definition)
 493 is a relative measure of long-term performance and that non-zero values do not
 494 necessarily imply net heat gain in a given 24h period. For example, heat gained on a
 495 cloudy day following several warm sunny days could well be less than the amount of
 496 heat lost during a subsequent cool night, even with relatively high collection, retention
 497 and diurnal thermal efficiencies.

$$498 \quad Q_{T,24max} = \eta_{T,col} \cdot A_1 \cdot H_{col} \quad \text{Equation 19}$$

$$499 \quad Q_{T,24min} = \eta_{T,col} \cdot \eta_{T,ret} \cdot A_1 \cdot H_{col} \quad \text{Equation 20}$$

$$500 \quad \eta_{T+E,24} = \eta_{T,24} + \eta_{E,24} = \eta_{T,col} \cdot \eta_{T,ret} + \frac{1}{t_{col}} \int_{t=0}^{t=t_{col}} \frac{q_E}{G \cdot A_1} \quad \text{Equation 21}$$

501 Table 2 summarises performance values reported in previous experimental studies on
 502 ICSSWH collector prototypes to serve as benchmarks for the devices examined in this
 503 and future studies. A confusing variety of metrics and test methodologies are reported
 504 in the literature, but most can be readily interpreted and converted into $\eta_{T,col}$, $\eta_{T,ret}$,
 505 and $U_{r,sys}A_{sys}$ parameters according to the definitions given above. It is important to
 506 ensure that the solar thermal condition is properly accounted for when comparing
 507 reported collection efficiencies because $\eta_{T,col}$ inherently reduces with increasing N. Test
 508 duration and tank-to-ambient temperature difference must be borne in mind when
 509 comparing retention efficiencies because $\eta_{T,ret}$ inherently reduces with increasing t_{ret}
 510 and ΔT_{3a} . Likewise, comparisons between heat loss coefficients must be made with
 511 caution because there is a lack of consistency concerning definitions for reference areas
 512 (these are variably reported based on the absorber, aperture, or whole envelope area)
 513 and because $U_{sys}A_{sys}$ inherently increases in proportion to the physical size of the
 514 ICSSWH. To enable fair comparisons in relation to heat retention performance, we
 515 propose two new heat loss coefficient metrics, one of which is referenced to stored
 516 water volume ($U_{r,sys}A_{sys}/u$) and the other of which is referenced to the effective aperture
 517 area ($U_{r,sys}A_{sys}/A_1$). The latter has the advantage of being broadly equivalent to $F \cdot U_L$
 518 values reported for conventional solar water heating collectors whereas the former is
 519 very useful when drawing comparisons between ICSSWH collectors with very different
 520 storage tank sizes and shapes. It should be noted that the data reported in Table 2 is
 521 drawn from a variety indoor and outdoor tests for which the influences of variables
 522 such as wind speed (which affects heat losses) and solar incidence angle (which affects
 523 optical losses) cannot easily be determined. Data in Table 2 suggests a state-of-the-
 524 art benchmark ICSSWH collection efficiency of $\eta_{T,col} \approx 60\%$ at $N \approx 0.035 \text{m}^2 \text{K} \cdot \text{W}^{-1}$

525 (comparable to efficiencies achieved by basic conventional solar thermal collectors,
526 refer to Figure 3) and state-of-the-art benchmark heat loss coefficients of
527 $U_{r,sys}A_{sys}/A_1 \approx 1 \text{ W}\cdot\text{m}^{-2}\text{K}^{-1}$ and $U_{r,sys}A_{sys}/u \approx 10 \text{ W}\cdot\text{m}^{-3}\cdot\text{K}^{-1}$ at $\Delta T_{3a} \approx 25^\circ\text{C}$ (equivalent to a
528 100L cube shaped tank fully insulated on all sides with 30mm insulation of conductivity
529 $k=0.025 \text{ W}\cdot\text{m}^{-1}\text{K}^{-1}$).

530

531 **Table 2: Performances of ICSSWH collectors reported in the literature**

ICSSWH description	Solar thermal collection efficiency	Over-night heat retention efficiency	Test duration	Overall heat loss coefficient	Effective aperture area	Water storage vessel volume	Aperture specific heat loss coefficient	Volume specific heat loss coefficient
	$\eta_{T,col}$	$\eta_{T,ret}$	$t_{col} + t_{ret}$	$U_{r,sys}A_{sys}$	A_1	u	$\frac{U_{r,sys}A_{sys}}{A_1}$	$\frac{U_{r,sys}A_{sys}}{u}$
	(%)	(%)	(hours)	($\text{W}\cdot\text{K}^{-1}$)	(m^2)	(L)	($\text{W}\cdot\text{m}^2\text{K}^{-1}$)	($\text{W}\cdot\text{m}^3\text{K}^{-1}$)
Near-triangular trapezoidal prism tank, single glazed, 25mm insulation. Thermosiphonically coupled absorber channel, thermal diode reverse flow stop valve. (Mohamad, 1997)	53*	66	12+12	4*	0.55	100	7.3*	40*
Semi-flat trapezoidal tank, double (?) glazed, 50mm insulation. Thermosiphonically coupled absorber channel, thermal diode reverse flow stop valve. (Faiman et al., 2001)	34	84	11+8.5	2.8	1.15	120	2.4	23
Horizontal cylindrical tank, two-part CPC reflector, single glazed. (Tripanagnostopoulos et al., 2002)								
<i>STS-1A & 2A: Single tank</i>	41	58	12+12	5.3	0.95	100	5.6	53
<i>STS-1B & 2B: Modified reflector</i>	48	57	12+12	5.5	0.95	100	5.8	55
<i>DTS-2B: Double tanks, modified reflector</i>	50	50	12+12	6.7	0.95	100	7.1	67
Cylindrical tank, selective coating, two-part CPC reflector, single glazed, insulated. (Smyth et al., 2003)								
<i>A2: Basic design</i>	52	45	8+16	4.2	0.92	57	4.6	74
<i>A4: Internal perforated sleeve added</i>	58	53	8+16	3.4	0.92	57	3.7	60
<i>A8: extra insulation added</i>	59	61	8+16	4	0.92	85	4.3	47
Close-coupled tubular absorber on top of a flat cuboid tank with bulbous head. Tank fully enclosed with 40mm insulation. (Sopian et al., 2004)								
1: <i>Free thermosiphonic flow</i>	45	18	8+16	40.9	2.30	329	17.8	124
2: <i>Thermal diode reverse flow stop valve</i>	45	52	8+16	15.6	2.30	329	6.8	47
Double horizontal cylindrical tanks, three-part CPC reflector, single glazed, insulated. Tripanagnostopoulos & Souliotis (2006)								
<i>DTS-B2 reflector design variant</i>	55	53	12+12	6.5	1.01	107	6.4	61
<i>DTS-C2 reflector design variant</i>	46	59	12+12	5.5	0.75	107	7.3	51
Horizontal cylindrical tank-in-tank, selective coating, two-part CPC reflector, single glazed, insulated. Air-filled annulus. (Souliotis et al., 2011)	33	66	12+12	1.5	0.83	44	1.8	34

Cuboid tank, selective coating on underside, 50mm insulation elsewhere. Single glazed aperture with reflectors (1.8x CPC, reverse circular & straight) directing light onto inverted absorber. (Smyth et al., 2005)									
1: No baffles in reflector	43	86	8+16	0.81	0.36	38	2.3	21	
2: Two full-width transparent baffles	40	92	8+16	0.45	0.36	38	1.3	12	
7: One half-width transparent baffle	46	85	8+16	0.84	0.36	38	2.3	22	
Horizontal cylindrical tank, selective coating, two-part CPC reflector, glazed, insulated. (Souliotis et al., 2013)									
3A: Single glazing	54	61	12+12	4.85	1.48	102	3.3	48	
3B: Double glazing	53	65	12+12	4.2	1.48	102	2.8	41	
Horizontal cylindrical tank-in-tank, selective coating, two-part CPC reflector, single glazed, insulated. Evacuated annulus part-filled with water to form a thermal diode (Souliotis et al., 2017)									
Starting pressure 86mbar	29	74	12+12	1.29	0.83	44	1.6	29	
Starting pressure 998mbar	31	68	12+12	1.66	0.83	44	2.0	38	
Vertical cylindrical tank-in-tank, matt black, transparent plastic cylindrical cover, insulated ends. Evacuated annulus (38mbar) with pumped thermal diode. (Smyth et al., 2018)	36*	61	6+18	0.9	0.32	28	2.9	32	
Horizontal cylindrical tank-in-tank, matt black, transparent plastic cylindrical cover, insulated ends. Evacuated annulus part-filled with water to form a thermal diode (Muhumuza et al., 2019)									
1: Aluminium outer vessel, no capillary	28*	25	6+18	1.5	0.24	17	6.1	88	
2: Stainless steel outer vessel + capillary	31*	40	6+18	1	0.24	17	4.1	59	
3: As variant 2 but longer vessels	29*	48	6+18	1.3	0.40	28	3.2	46	
Horizontal rectangular tank, matt black, insulated on 5 sides with double glazed cover (Harmim (2019)	47	93	12+12	2.6	1.13	60	2.3	43	
Benchmarks									
Minimum reported in literature	28						1.3	12	
Average reported in literature	43						4.6	49	
Maximum reported in literature	59						17.8	124	
Targets for ICSSWH development	60						1.0	10	

532 Collection efficiencies reported in the table relate to an average daily solar thermal condition of $N=0.035\pm 0.005 \text{ m}^2\text{K}\cdot\text{W}^{-1}$. Retention efficiencies and
533 heat loss coefficients reported in the table relate to a normalised stored water temperature of $\Delta T_{3a} = 25\pm 10^\circ\text{C}$ (averaged over the retention period).
534 Exceptions where data relates to $N \approx 0.01 \text{ m}^2\text{K}\cdot\text{W}^{-1}$ and $\Delta T_{3a} \approx 10^\circ\text{C}$ are marked with asterisk*. Reported values of A_1 relate to the transparent
535 aperture area (excluding external framing elements) which is typically the same as the absorber area for non-concentrating ICSSWH devices.

536

537 **2.6 Planar Liquid-Vapour Thermal Diodes**

538 A thermal diode is a unidirectional heat transfer device that operates in a manner
539 analogous to an electrical semiconductor diode by offering low resistance (thermal
540 conductance) in one direction and high resistance (thermal insulation) in the other.
541 Thermal diode devices have been used to successfully reduce heat loss via reverse flows
542 in thermosiphonic solar water heaters (one-way valves employed by Mohamad, 1997;
543 Faiman et al., 2001; Sopian et al., 2004), to promote stratification in hot water storage
544 tanks (Smyth et al., 1999 and Rhee et al., 2010), and to reduce overnight heat losses
545 from ICSSWH absorbers (De Beijer, 1998; Quinlan, 2010; Souliotis et al., 2011&2017;

546 Smyth et al., 2015a&b, 2017, 2018, 2019; Pugsley et al., 2016 & 2017; Muhumuza et
547 al., 2019a&b and 2020).

548 Planar Liquid-Vapour Thermal Diodes (PLVTD) consist of two parallel plates of area
549 $A=yz$ separated by a cavity of depth x which contains a quantity of working fluid
550 maintained in a thermodynamic state close to saturation (Pugsley et al., 2019 & 2020).
551 During forward mode operation, wetting of the hottest plate (evaporator) through
552 contact with the liquid working fluid generates vapour, which then migrates to the
553 colder plate (condenser) where it releases its latent heat and generates condensate to
554 complete the cycle. During reverse mode operation, the hottest plate is kept dry so
555 that no vapour can be generated, no latent heat transfer occurs, and the partially
556 evacuated cavity acts as an insulator (see Figure 4). Requirements, functions and
557 interactions of the main PLVTD components can be summarised as follows, based on
558 Pugsley et al. (2017 & 2020):

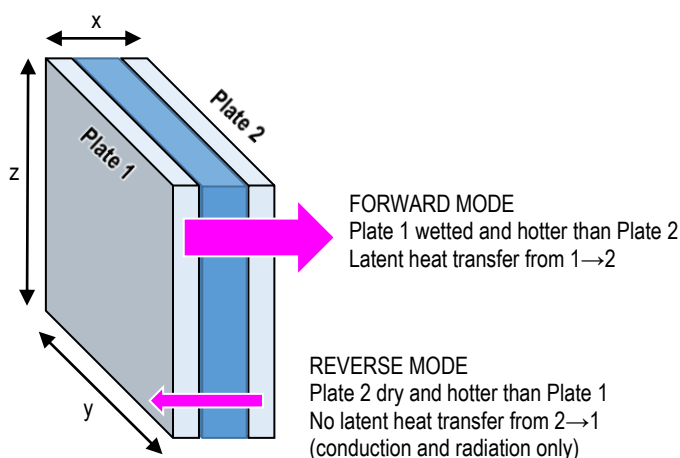
- 559 • **Evaporator and condenser plates** should be formed of thermally conductive
560 material and should be as thin as possible to maximise forward mode heat
561 transfer. Choice of plate thickness is also governed by the inherent need to
562 prevent structural deformation caused by implosion forces associated with the
563 combination of cavity vacuum and external atmospheric pressure. Internal
564 supporting structure is generally required in large PLVTDs. Hermetic sealing is
565 required to prevent infiltration of non-condensable gases.
- 566 • **Cavity sidewalls and internal structure** should have low thermal
567 conductivity to minimise bridging that would otherwise cause unwanted reverse
568 mode heat transfer. These elements must provide sufficient structural strength
569 to prevent deformation and should be formed of low-outgassing materials to
570 avoid risk of vacuum degradation (also applies to plates and seal materials).
571 Internal structures must not significantly impede vapour flows between the
572 plates in order to avoid impairing forward mode heat transfer.
- 573 • **Working fluid** selection considerations include saturation pressure at operating
574 temperature, specific heat capacity, liquid & vapour thermal conductivities,
575 liquid & vapour viscosities, latent heat of vaporisation, cost, flammability,
576 toxicity, global warming and ozone depletion potential. Water appears to be a
577 suitable fluid. Determination of required quantity involves consideration of plate
578 area, cavity volume, the need to minimise thermal inertia, and the need to avoid
579 evaporator dry-out at high temperatures. Working fluid reservoirs should be
580 designed to prevent thermal bridging between the plates.

581 • **Evaporator wetting and condensate return mechanisms** must ensure
582 continuous and uniform working fluid flows during forward mode operation and
583 should preferably maintain dry plates in reverse mode. Evaporator hydrophilicity
584 and condenser hydrophobicity are important considerations. Evaporator wetting
585 can be achieved by a variety of active (eg pumped falling film or spray) or
586 passive (eg capillary wick or pockets) techniques. Consideration should be given
587 to parasitic energy consumption by pumps in active systems.

588 Experimental and theoretical work by Pugsley et al. (2016, 2017, 2019 & 2020)
589 demonstrated that large vertical PLVTDs ($A=0.98\text{m}^2$ and $x=70\text{mm}$ deep) suitable for
590 integration in façade mounted ICSSWH collectors can be realised to achieve reverse
591 mode insulation of $U_r < 2 \text{ W}\cdot\text{m}^{-2}\text{K}^{-1}$ and forward mode heat transfer in the range
592 $50 < U_f < 900 \text{ W}\cdot\text{m}^{-2}\text{K}^{-1}$. Reverse mode insulation is determined by PLVTD dimensions
593 such that thermal conductance decreases with increasing depth. Forward mode heat
594 transfer is highly dependent upon PLVTD operating conditions such that thermal
595 conductance increases with increasing temperature and increasing heat flux but is
596 relatively insensitive to PLVTD dimensions.

597 Using a vertical PLVTD as the connecting element between PV cells and water storage
598 tank in a BIPV-ICSSWH facade system has the potential to not only reduce ICSSWH
599 heat losses by improving tank insulation, but also to improve thermal and electrical
600 collection efficiencies by improving heat transfer. Given that PLVTDs essentially act as
601 heat spreaders (Boreyko and Chen, 2013) there is also potential for electrical efficiency
602 improvements associated with improved PV cell temperature uniformity.

603



604

605

606 **Figure 4: Schematic diagram of a PLVTD**

607

608

609 **3 Theoretical understanding of a BIPV-PLVTD-ICSSWH**

610 **3.1 Energy balance model**

611 The fundamental physical arrangement of the BIPV-PLVTD-ICSSWH device proposed
612 in Figure 1 can be represented by the lumped parameter model shown in Figure 5 and
613 the equivalent resistance network shown in Figure 6. The model describes how the
614 input solar flux (G) is absorbed by the PV cells (at temperature T_0) where it is converted
615 to thermal energy and electrical energy. The thermal power is either lost (q_{0a}) to the
616 ambient environment (at temperature T_a) or transferred through the thermal diode
617 (q_{03}) to heat the water storage tank (at temperature T_3) where it becomes available
618 for delivery to thermal loads (q_T). Heat transferred from the absorber to the stored
619 water passes through the diode (R_{12}) and storage tank mantle (R_{23}) thermal
620 resistances. Some of the solar heat gained by the tank is lost through the insulated
621 tank sidewalls and back plate (q_{3a} through $R_{3i}+R_{ia}$). Heat losses through the insulated
622 thermal diode sidewalls (q_{4a}) are neglected as these are small by comparison. Absorber
623 heat losses (q_{1a}) pass through the absorber laminate (R_{15}), transparent cover (R_6),
624 airgap (R_{56}) and ambient (R_{6a}) thermal resistances which act in series to determine the
625 overall absorber loss resistance (R_{1a}). It is assumed that each element is isothermal
626 and that heat fluxes are constant across the plane of each element. The amount of
627 electrical power produced by the PV cell array ($q_E=I_{PV}.V_P$) is dependent upon the
628 irradiance (G); the pump and load electrical resistances (R_P+R_{load}); and the PV cell
629 array electrical characteristics (represented by R_{PV}) which are themselves dependent
630 upon the cell material properties and temperature. Some of the electrical power
631 generated by the PV is delivered to a small pump (q_p) which distributes a working fluid
632 film to wet the PLVTD evaporator and the remainder (q_E) is available to serve applied
633 electrical loads (R_{load}). It is assumed that all electrical energy used to drive the pump
634 is eventually converted to heat which is added to the stored water ($q_{p,T}=q_{p,E}=I_P.V_P$).

635 Collection behaviour of the BIPV-PLVTD-ICSSWH can be modelled by considering the
636 energy balances within the absorber laminate (Equation 22), storage tank (Equation
637 23), and connected electrical load (Equation 24) by accounting for the transparent
638 cover transmissivity (τ); the absorber surface area (A_1) and absorptivity (α); and the
639 electrical currents flowing from the PV output (at voltage V_P) to ground through the
640 PV, pump and load (I_{PV} , I_P and I_{load} respectively). It should be noted that the optical
641 efficiency ($\tau\alpha$) is dependent upon the solar incidence angle. Substituting Equation 24
642 into Equation 1, and the resultant expression into Equation 23, yields Equation 25
643 which describes overall thermal power output. In cases where the pump is fed from an
644 external power supply (as occurred for solar simulator laboratory tests described in
645 Part 2 of 2) the overall thermal power output is described by Equation 26.

$$646 \quad \tau \cdot \alpha \cdot G \cdot A_1 = q_E + q_P + q_{03} + q_{0a} \quad \text{Equation 22}$$

$$647 \quad q_T = q_{03} + q_P - q_{3a} \quad \text{Equation 23}$$

$$648 \quad q_E = q_{PV} - q_P = V_P(I_{PV} - I_P) = V_P I_{load} \quad \text{Equation 24}$$

$$649 \quad q_T = \tau \cdot \alpha \cdot G \cdot A_1 - V_P I_{load} - q_{0a} - q_{3a} \quad \text{Equation 25}$$

$$650 \quad q_T = \tau \cdot \alpha \cdot G \cdot A_1 - V_P(I_{PV} + I_P) - q_{0a} - q_{3a} \quad \text{Equation 26}$$

651 Inspection of the thermal resistance network in Figure 6 indicates that absorber heat
 652 loss (q_{0a}) can be expressed in terms of normalised absorber temperature ($\Delta T_{0a}=T_0-T_a$)
 653 and the series thermal resistances $R_{05}+R_{56}+R_6+R_{6a}$ to create Equation 27. Tank heat
 654 loss (q_{3a}) and tank heat gain (q_{03}) can likewise be expressed in terms of normalised
 655 tank temperature ($\Delta T_{3a}=T_3-T_a$) and the absorber-to-tank temperature difference
 656 ($\Delta T_{03}=T_0-T_3$) together with relevant thermal resistances to create Equations 28 & 29.

$$657 \quad q_{0a} = \frac{T_0 - T_a}{R_{05} + R_{56} + R_6 + R_{6a}} = \frac{\Delta T_{0a}}{R_{0a}} \quad \text{Equation 27}$$

$$658 \quad q_{3i} = \frac{T_3 - T_a}{R_{3i} + R_{ia}} = \frac{\Delta T_{3a}}{R_{3a}} \quad \text{Equation 28}$$

$$659 \quad q_{03} = \frac{T_0 - T_3}{R_{01} + R_{12} + R_{23}} = \frac{\Delta T_{03}}{R_{03}} \quad \text{Equation 29}$$

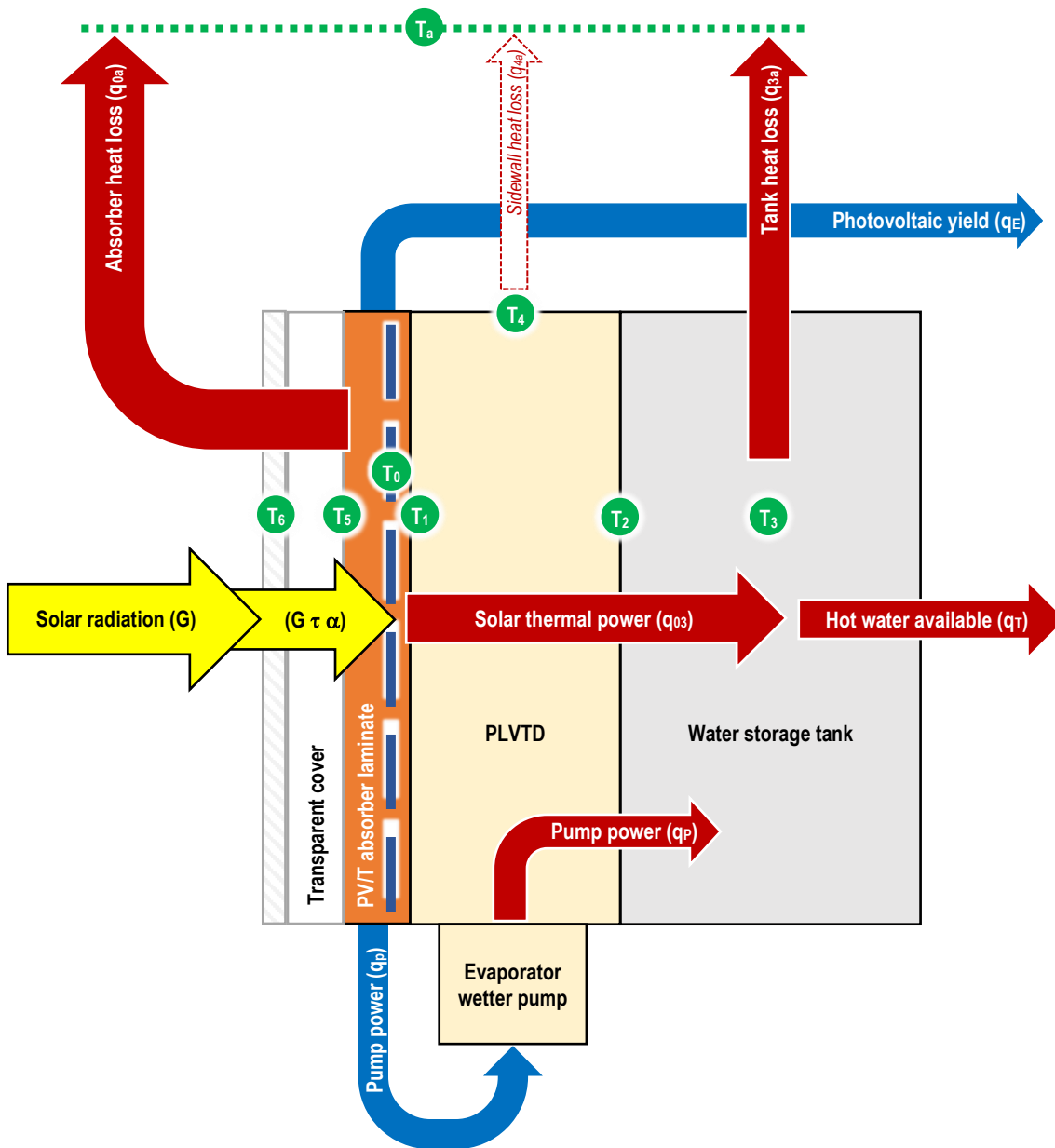
660 During collection, absorbed solar radiation is converted to heat and electricity in
 661 accordance with the absorber laminate energy balance. Substituting Equations 27 &
 662 28 into Equation 25; and substituting Equations 28 & 29 into Equation 23; yields
 663 Equations 30 & 31 which describe the maximum amount of thermal power that the
 664 tank can deliver over a sustained period. Substituting Equations 27 & 29 into
 665 Equation 22 and rearranging into Equation 32 allows the absorber temperature (T_0) to
 666 be evaluated. Substituting Equation 30 into Equation 9 allows the solar thermal
 667 collection efficiency to be evaluated according to Equation 33. It should be noted that
 668 the term $V_P I_P$ is only relevant when pumping power for the PLVTD evaporator wetter is
 669 supplied by the PV cells.

$$670 \quad q_T = \tau \cdot \alpha \cdot G \cdot A_1 - V_P I_{load} - \frac{T_0 - T_a}{R_{0a}} - \frac{T_3 - T_a}{R_{3a}} \quad \text{Equation 30}$$

$$671 \quad q_T = \frac{T_0 - T_3}{R_{03}} + V_P I_P - \frac{T_3 - T_a}{R_{3a}} \quad \text{Equation 31}$$

$$672 \quad T_0 = \frac{(R_{03} R_{0a})(\tau \cdot \alpha \cdot G \cdot A_1 - q_E - q_P) + T_a R_{03} + T_3 R_{0a}}{R_{03} + R_{0a}} \quad \text{Equation 32}$$

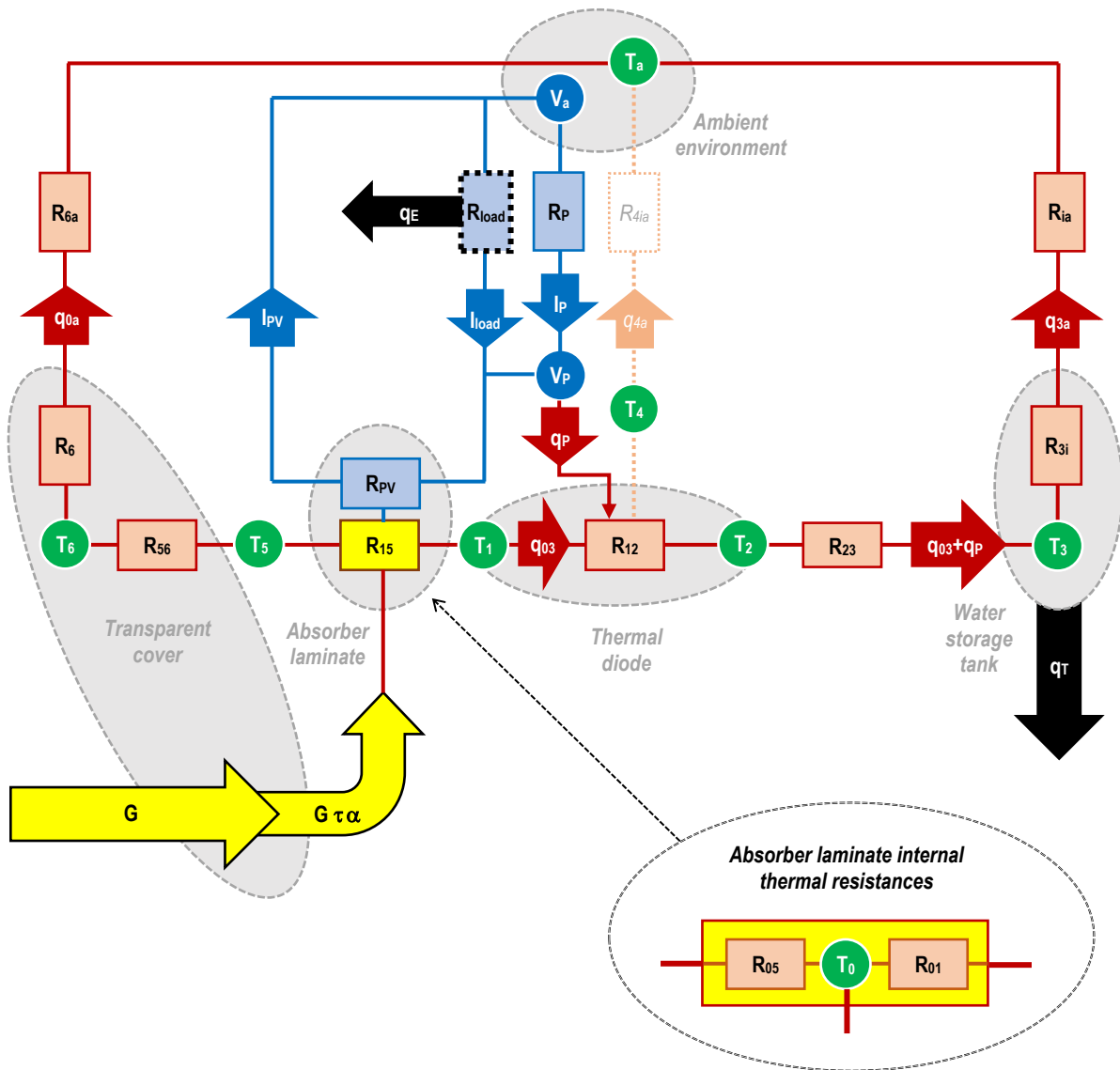
$$673 \quad \eta_T = \frac{(T_0 - T_3)/R_{03} - (T_3 - T_a)/R_{3a} + (V_P I_P)}{G \cdot A_1} \quad \text{Equation 33}$$



674
675

T_a	Ambient environmental temperature	G	Incident solar radiation flux
T_0	Photovoltaic cell temperature	$G\tau\alpha$	Absorbed solar radiation
T_1	Temp. of absorber laminate substrate and evaporator	q_{03}	Thermal power transferred from the absorber to the water storage tank through the thermal diode
T_2	Temperature of condenser plate and tank mantle	q_T	Net rate of heat gained by the stored water bulk
T_3	Temperature of water bulk stored in the tank	q_{0a}	Absorber heat loss rate
T_4	Thermal diode sidewall temperature	q_{3a}	Rate of heat loss from the back and sides of the water storage tank not covered by the thermal diode
T_5	Absorber laminate surface temperature	q_E	Net electrical power yielded
T_6	Transparent cover temperature	q_P	Electrical power consumed by the evaporator wetter pump which is then all converted to heat

676 *Figure 5: Lumped parameter model of a BIPV-PLVTD-ICSSWH*
677



678
679

$G\tau\alpha$	Absorbed solar radiation	V_P	Evaporator wetter pump supply voltage
q_{T+E}	Thermal and electrical power available for use	V_a	Earth electrical potential (zero voltage)
q_{0a}	Heat lost from the absorber	I_{PV}	Current delivered by the photovoltaic module
q_{03}	Solar thermal power transferred to tank	I_{load}	Current drawn by the load
q_{3a}	Heat lost from the water storage tank	I_P	Current drawn by the evaporator wetter pump
q_P	Wetter pump power (electrical becomes thermal)	R_{load}	Electrical load connected to photovoltaic module
R_{1a}	Overall absorber heat loss thermal resistance	R_{PV}	Electrical resistance of photovoltaic module
R_{23}	Water storage tank mantle thermal resistance	R_P	Electrical load of the evaporator wetter pump
$R_{3i}+R_{ia}$	Water storage tank back and side insulation	T_a	Ambient environmental temperature
R_{4ia}	Thermal diode sidewall insulation (assumed infinite)	T_0	Photovoltaic cell temperature
R_{56}	Air gap between absorber and transparent cover	T_1	Absorber substrate & evaporator plate temperature
R_6	Transparent cover thermal resistance	T_2	Temperature of condenser plate and tank mantle
R_{6a}	External air convection & radiation to ambient	T_3	Temperature of water bulk stored in the tank
R_{15}	Absorber laminate thermal resistance	T_4	Thermal diode sidewall temperature
R_{01}	Thermal resistance of laminate behind cells	T_5	Absorber laminate surface temperature
R_{05}	Thermal resistance of laminate in front of cells	T_6	Transparent cover temperature

680 **Figure 6: Thermal and electrical resistance network for a BIPV-PLVTD-ICSSHW**

$$U_{r,sys} = \frac{1}{A_{sys}} \left[\frac{1}{R_{3a}} + \frac{1}{(R_{03}+R_{0a})} \right] \quad \text{Equation 34}$$

$$\eta_{T,ret} = \frac{M \cdot c_p \Delta T_{3a[t=t_{col}]} - t_{ret} \left[\frac{(\bar{T}_{3[t_{ret}]} - \bar{T}_{0[t_{ret}]})}{R_{03}} - \frac{(\bar{T}_{3[t_{ret}]} - \bar{T}_{a[t_{ret}]})}{R_{3ia}} \right]}{M c_p (T_{3[t=t_{col}]} - T_{a[t=t_{col}]})} \quad \text{Equation 35}$$

$$F = \frac{R_{0a}}{R_{03}+R_{0a}} \left[\frac{G \cdot A_1 - q_E}{G \cdot A_1} \right] \quad \text{Equation 36}$$

$$F \cdot U_L = \frac{1}{A_1} \left[\frac{1}{R_{3a}} + \frac{1}{(R_{03}+R_{0a})} \right] \left[\frac{G \cdot A_1 - q_E}{G \cdot A_1} \right] \quad \text{Equation 37}$$

685 At night when there is no solar radiation ($G=q_E=q_P=0$) the network on Figure 6
 686 simplifies somewhat because the electrical elements become inactive and there is no
 687 solar flux component. The tank loses heat to the absorber at the same rate as the
 688 absorber loses heat to the ambient such that Equation 22 simplifies to $q_{03}+q_{0a}=0$ and
 689 the electrical and optical terms of Equations 30-32 become zero. The heat loss
 690 coefficient can be expressed in terms of thermal resistances according to Equation 34.
 691 Likewise, combining Equations 14 & 31 yields Equation 35 which enables the heat
 692 retention efficiency to be evaluated. Heat removal factor can be evaluated using
 693 Equation 36 (obtained from inspection of Figure 6) or Equation 37 (obtained by
 694 substituting Equation 34 into Equation 10). It is interesting to note that in the case of
 695 a thermal-only collector ($q_E=0$), inspection of Equation 36 confirms that $F \rightarrow 1$ when
 696 $R_{0a} \rightarrow \infty$ or $R_{03} \rightarrow 0$; $F \rightarrow 0$ when $R_{03} \rightarrow \infty$ or $R_{0a} \rightarrow 0$; and $F=0.5$ when $R_{03}=R_{0a}$.

697 **3.2 Thermal diodicity and its effect on performance**

698 Diodicity coefficient (ζ) is a dimensionless measure of thermal rectification and is a
 699 useful performance measure for thermal diodes. It is commonly defined according to
 700 Equation 38 as a scalar based on the apparent thermal conductivities (k) of the device
 701 in forward (f) heat transfer mode and reverse (r) insulation modes. It can alternatively
 702 be written in terms of thermal power (q), heat flux (q/A), thermal conductance
 703 ($U=k/x$), or reciprocal thermal resistance ($1/R=UA$). A reasonable target for diodicity
 704 of PLVTDs in ICSSWH applications would be $\zeta > 99\%$ to replicate absorber transparent
 705 cover arrangements in ICSSWH devices where the insulation of high quality double
 706 glazing unit is $U \approx 1.2 \text{ W} \cdot \text{m}^{-2} \text{ K}^{-1}$ (Twidell & Weir, 2006) and heat transfer across the
 707 absorber should be $U > 200 \text{ W} \cdot \text{m}^{-2} \text{ K}^{-1}$ (Dupeyrat et al., 2011, Deng et al., 2019).

$$\zeta = \frac{k_f - k_r}{k_f + k_r} \quad (0 \leq \zeta \leq 1) \quad \text{Equation 38}$$

709 Heat transfer through the diode component in a BIPV-PLVTD-ICSSWH device is
 710 represented in the lumped parameter model by thermal resistance ($R_{12}=1/U_{12}A_1$).

711 Inspection of Figure 6 highlights that this is a key component in the absorber-to-store
712 thermal resistance $R_{03}=R_{01}+R_{12}+R_{23}$ which has a major influence upon the absorber
713 temperature (T_0), heat removal factor (F) and heat loss coefficients (U_L and U_{sys}) as
714 described by Equations 29-37. Given that the solar thermal and photovoltaic collection
715 efficiencies are dependent upon $F \cdot U_L$ and T_0 respectively, and that the heat retention
716 behaviour is determined by $U_{r,sys}$, it is very clear that the U_{12} of the PLVTD has a major
717 influence upon performance. To quantify this, the model described in the preceding
718 sections has been used to examine how thermal diode resistances affect the
719 performance of a notional BIPV-PLVTD-ICSSWH with $A_1=1\text{m}^2$ collection area, $u=100\text{L}$
720 storage tank, and the component properties set out in Table 3.

721 Pugsley et al. (2019 & 2020) proposed and validated calculation methods and a
722 parametric design approach for evaluating the thermal resistances exhibited by a
723 PLVTD and developed a working prototype. Tests demonstrated that the prototype
724 ($A=0.98\text{m}^2$ and $x=70\text{mm}$ deep) achieved reverse mode insulation of
725 $U_{r,12}=1.7 \text{ W}\cdot\text{m}^{-2}\text{K}^{-1}$ (equivalent to $R_{12}=0.6 \text{ K/W}$) and typical forward mode heat transfer
726 of $U_{f,12}=38 \text{ W}\cdot\text{m}^{-2}\text{K}^{-1}$ (equivalent to $R_{12}=0.03 \text{ K/W}$) corresponding to diodicity of
727 $\zeta \approx 90\%$. Analysis concluded that an order of magnitude increase in forward mode
728 performance could feasibly be realised by improving evaporator wetting uniformity.

729 Equations 5-10, 32 & 37 have been used to calculate the results on Figures 7 & 8 which
730 illustrate how varying forward mode thermal conductance ($1 < U_{f,12} < 1000 \text{ W}\cdot\text{m}^{-2}\text{K}^{-1}$,
731 equivalent to $0.001 < R_{12} < 1 \text{ K/W}$) affects the solar thermal collection efficiency ($\eta_{T,col}$)
732 and PV/T performance ratio (PR_{T3}). Low diode thermal conductance impairs absorber-
733 to-tank heat transfer causing high absorber temperatures which increase heat losses
734 (thus poor solar thermal collection efficiencies on Figure 7) and resistive electrical
735 losses (thus poor PV/T performance ratios on Figure 8). The degree to which low diode
736 thermal conductance adversely affects performance is dependent upon operating
737 conditions (G , T_a , T_3 , wind speed and electrical loads) but follows a similar trend for all
738 scenarios investigated. A notional "knee" point is apparent at $U_{f,12} \approx 100 \text{ W}\cdot\text{m}^{-2}\text{K}^{-1}$,
739 above which minimal performance benefit is gained for order of magnitude increases.
740 This knee corresponds closely to the point at which the zero-loss solar thermal
741 collection efficiencies of bare and covered collectors are approximately equal
742 ($\eta_{T,col} \approx 75\%$ at $N \approx 0 \text{ m}^2\text{K}\cdot\text{W}^{-1}$, no wind, no load).

743 The target benchmark solar thermal collection efficiency ($\eta_{T,col} \approx 60\%$ at
744 $N \approx 0.035 \text{ m}^2\text{K}\cdot\text{W}^{-1}$ and 2m/s wind speed, established in Table 2) is narrowly missed
745 ($\eta_{T,col} \approx 58\%$) for a covered BIPV-PLVTD-ICSSWH with $U_{f,12} \approx 100 \text{ W}\cdot\text{m}^{-2}\text{K}^{-1}$ but is

746 achievable under “no wind” conditions or if the diode thermal conductance is increased
747 to $U_{r,12} \approx 500 \text{ W}\cdot\text{m}^{-2}\text{K}^{-1}$. Whilst Figure 7 clearly shows that a transparent cover and air
748 gap is essential for achieving the solar thermal performance benchmark (this is
749 unachievable for a bare absorber, irrespective of $U_{r,12}$ or wind speed), the PR curves
750 on Figure 8 illustrate how the corresponding reduction in transmissivity reduces the
751 photovoltaic performance. PV/T performance ratios are worst when diode thermal
752 conductance is low, ambient temperature is high, and the collector is operating close
753 to the zero-loss solar thermal condition ($N=0$). The maximum achievable PR value is
754 limited by the PV cell packing factor which in the modelled case is $A_0/A_1=75\%$ but with
755 careful design could feasibly be $A_0/A_1 \approx 90\%$ to enable the benchmarks discussed in
756 Section 2.2 to be achieved.

757 Equations 15, 34 & 37 have been used to calculate the results shown in Figure 9 which
758 illustrate how varying the reverse mode thermal conductance
759 ($0.1 < U_{r,12} < 100 \text{ W}\cdot\text{m}^{-2}\text{K}^{-1}$, equivalent to $0.01 < R_{12} < 10 \text{ K/W}$) affects the overall heat
760 loss coefficient ($U_{r,sys}A_{sys}/u$) and the corresponding overnight heat retention efficiency
761 ($\eta_{T,ret}$ for a $t_{ret}=12\text{h}$ period). It is clear that overnight heat loss increases with increasing
762 diode thermal conductance. High $U_{r,12}$ values worsen vulnerability to wind induced heat
763 losses, especially when the bare absorber is exposed (no cover). On the basis of the
764 $U_{r,12}=1.7 \text{ W}\cdot\text{m}^{-2}\text{K}^{-1}$ reported by Pugsley et al. (2020), the results suggest that the BIPV-
765 PLVTD-ICSSWH design described by Figure 1 and Table 3 would achieve $\eta_{T,ret} > 80\%$
766 and a heat loss coefficient of $U_{r,sys}A_{sys}/u \approx 20 \text{ W}\cdot\text{m}^{-3}\text{K}^{-1}$ which is better than most of the
767 ICSSWHs encountered in the literature (see Table 2) but somewhat shy of
768 $U_{r,sys}A_{sys}/u < 10 \text{ W}\cdot\text{m}^{-3}\text{K}^{-1}$ benchmark target. Achieving the benchmark would require the
769 reverse mode PLVTD thermal conductance to be $U_{r,12} < 0.5 \text{ W}\cdot\text{m}^{-2}\text{K}^{-1}$. Further
770 interrogation of the model suggests that diode performance is relatively less important
771 if absorber heat loss is better controlled (double glazing and/or low emissivity surface
772 treatments) or if the tank is poorly insulated.

773

Table 3: Basis and assumptions for the modelled BIPV-PLVTD-ICSSWH

Quantity	Value	Unit	Basis
Volume of water in storage tank (u)	0.1	m ³	Typical tank size reported in literature
Aperture and absorber area (A_1)	1	m ²	Typical absorber size reported in literature
PV cell coverage of absorber area (A_0)	0.75	m ²	15 strings, each formed of 8 quarter-cell pieces (78x78mm)
Depth of PLVTD (x_{12})	70	mm	Dimension as discussed by Pugsley et al. (2020)
Depth of tank (x_3)	100	mm	Tank volume divided by absorber area
Absorber-to-ambient conductance (U_{5a} , bare) 5mm clear acrylic bonded to PV cells, no air gap	10.9*	W·m ⁻² K ⁻¹	Calculated from radiative & convective components as per Twidell & Weir (2006) assumes $T_5=50^\circ\text{C}$, $T_a=15^\circ\text{C}$, $\epsilon_5=0.8$, $\epsilon_6=0.9$
Absorber-to-ambient conductance (U_{5a} , covered) as above + 30mm air + 3mm clear acrylic cover	4.0*	W·m ⁻² K ⁻¹	Calculated from radiative & convective components as per Twidell & Weir (2006) assumes $T_5=50^\circ\text{C}$, $T_a=15^\circ\text{C}$, $\epsilon_5=0.8$
PV cell-to-absorber thermal conductance (U_{01})	400	W·m ⁻² K ⁻¹	Polymer bonding layer 0.5mm, thermal conductivity $k=0.2\text{ W}\cdot\text{m}^{-1}\text{K}^{-1}$
PV cell-to-air thermal conductance (U_{05})	40	W·m ⁻² K ⁻¹	Bonded transparent cover 5mm, thermal conductivity $k=0.2\text{ W}\cdot\text{m}^{-1}\text{K}^{-1}$
Tank wall-to-water thermal conductance (U_{23})	250	W·m ⁻² K ⁻¹	Natural convection heating of fluid adjacent to a vertical plate for $T_2=50^\circ\text{C}$, $T_3=49^\circ\text{C}$ equations recommended by Pugsley et al. (2020)
Tank insulation thermal conductance (U_{3a})	0.25	W·m ⁻² K ⁻¹	Rigid foam insulation 100mm, thermal conductivity $k=0.025\text{ W}\cdot\text{m}^{-1}\text{K}^{-1}$
Optical transmissivity (τ , bare) 5mm clear acrylic bonded to PV cells, no air gap	96	%	Estimated from optical reflection and absorption loss analysis offered by Kalogirou (2009) assuming normal incidence.
Optical transmissivity (τ , covered) as above + 30mm air + 3mm clear acrylic cover	88	%	Estimated from optical reflection and absorption loss analysis offered by Kalogirou (2009) assuming normal incidence.
Optical absorptivity of PV cells (α)	90	%	Value suggested by Dupeyrat et al. (2011) for mc-si PV cells
Optical emissivity of encapsulated PV cells (ϵ)	80	%	Nominal value for PV with bonded polymer cover, from Zondag (2008)
Standard power output of PV cell (q_{STC})	4.24	W	156x156mm pseudo square mc-si M-2BB solar PV cell (Bosch, 2010)
Voltage-temperature coefficient ($K_{V,T}$)	-0.37	%/K	156x156mm pseudo square mc-si M-2BB solar PV cell (Bosch, 2010)
Current-temperature coefficient ($K_{I,T}$)	+0.03	%/K	156x156mm pseudo square mc-si M-2BB solar PV cell (Bosch, 2010)

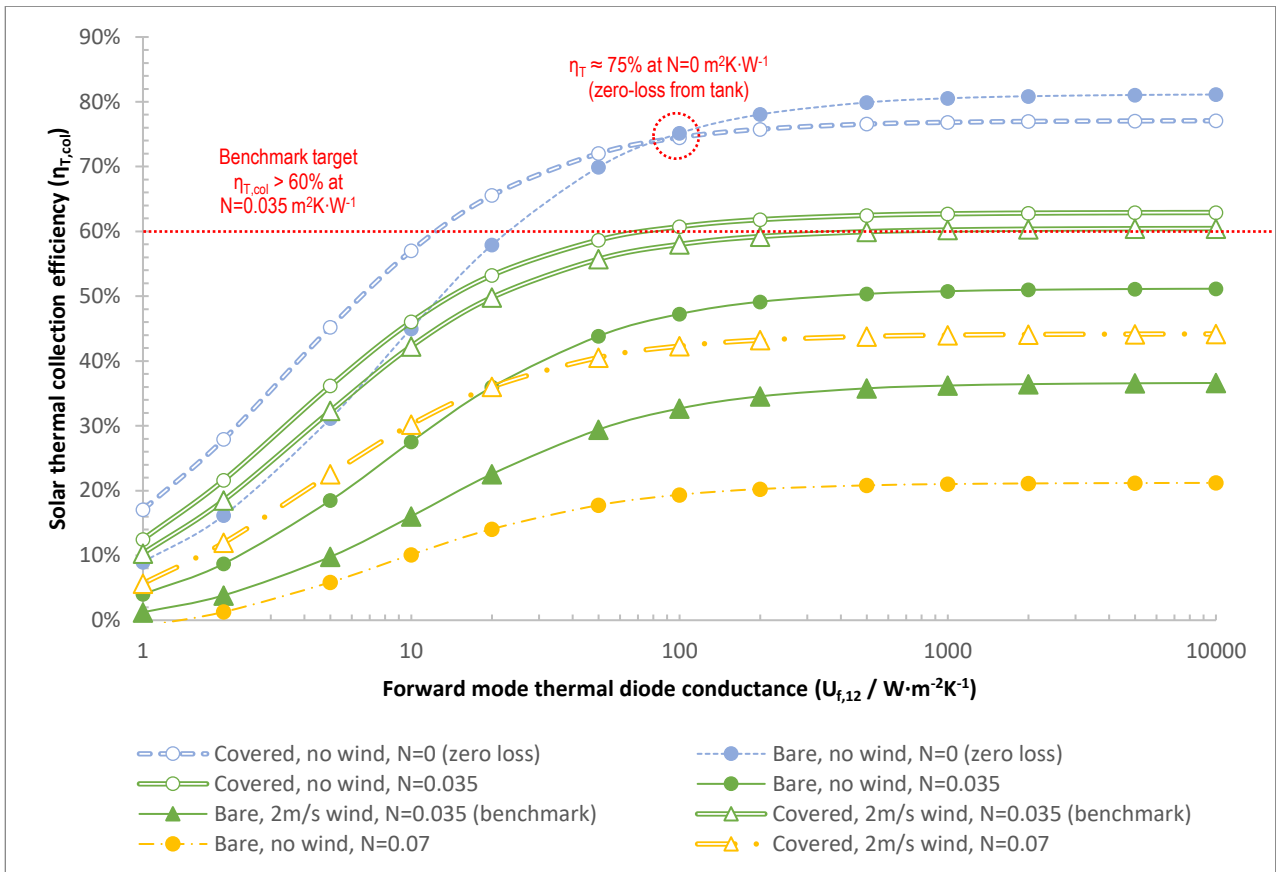
775

776

777

778

Values were chosen to be representative of the BIPV-PLVTD-ICSSWH prototype used for the experimental work (see Part 2 of 2). Stated values of U_{5a} marked with asterisk* relate to the "no wind" condition. Model accounts for effect of U_{5a} increasing with increasing local wind speed according to the relation offered by Twidell & Weir (2006). Calculations assume that evaporator wetter pump power is negligible ($q_p \approx 0$) and that the external electrical load has a resistance which enables operation at maximum power point.

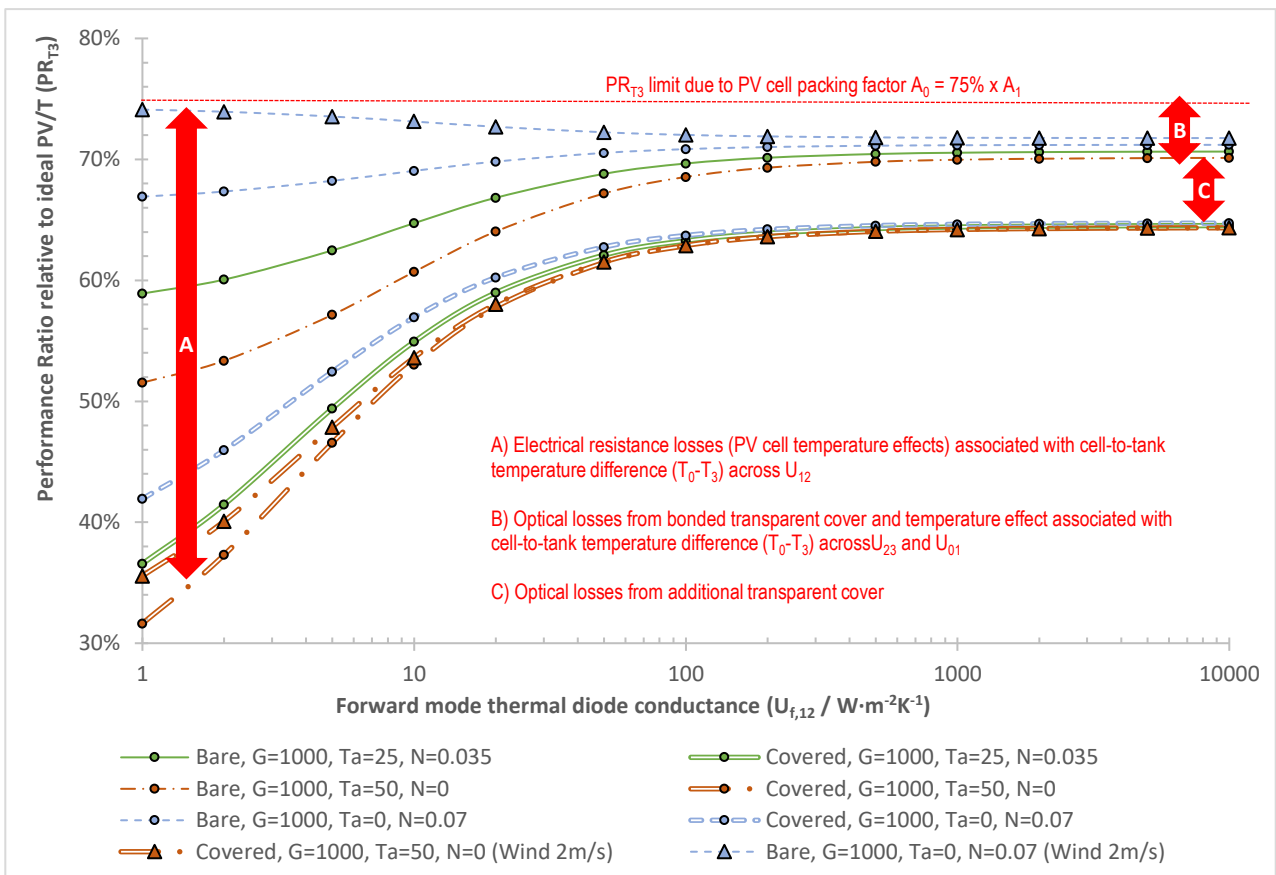


779

780

Figure 7: Dependence of solar thermal collection efficiency upon forward mode thermal diode conductance (zero electrical load $q_E=0$)

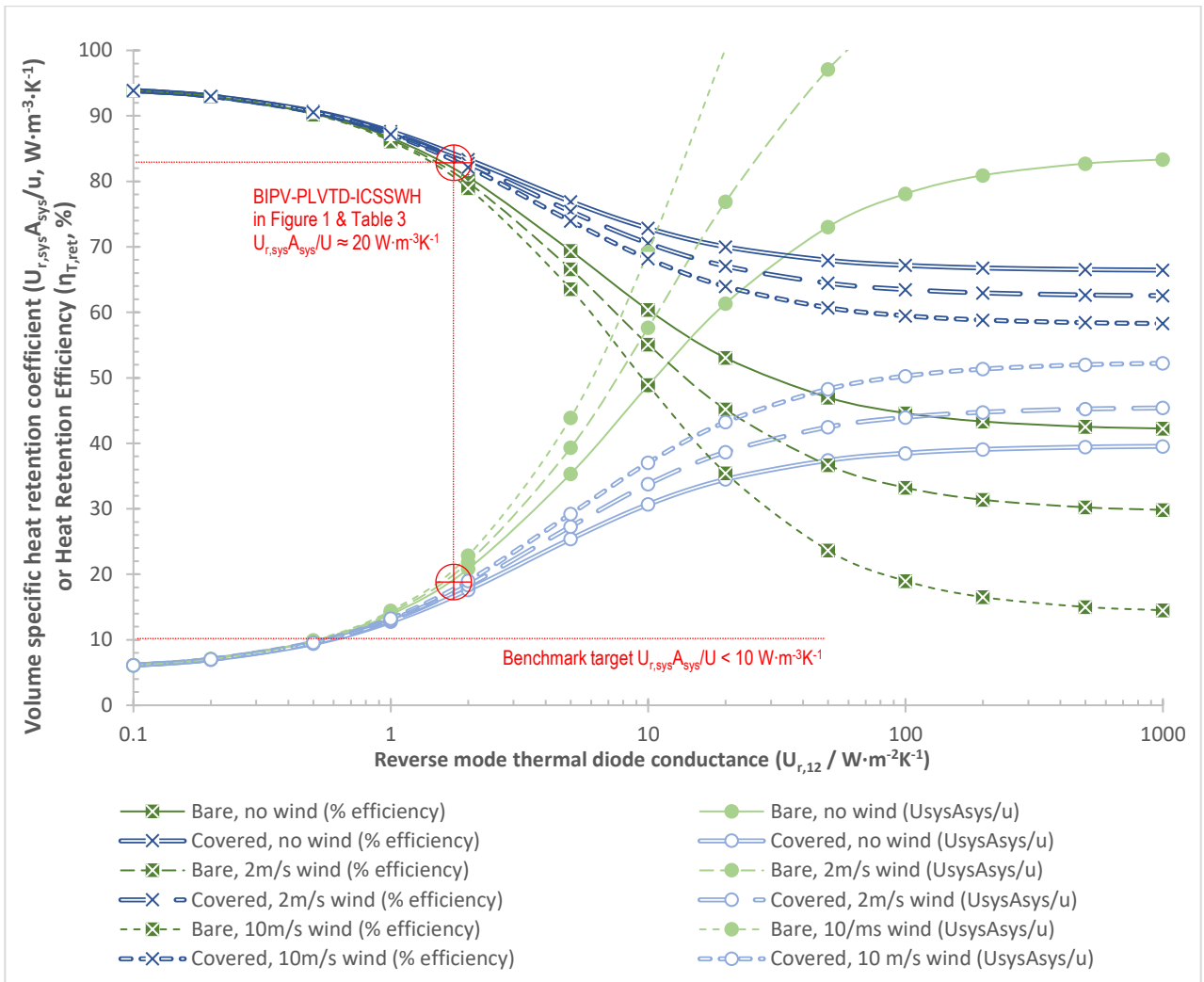
781



782

783

Figure 8: Dependence of PV/T Performance Ratio upon forward mode thermal diode conductance

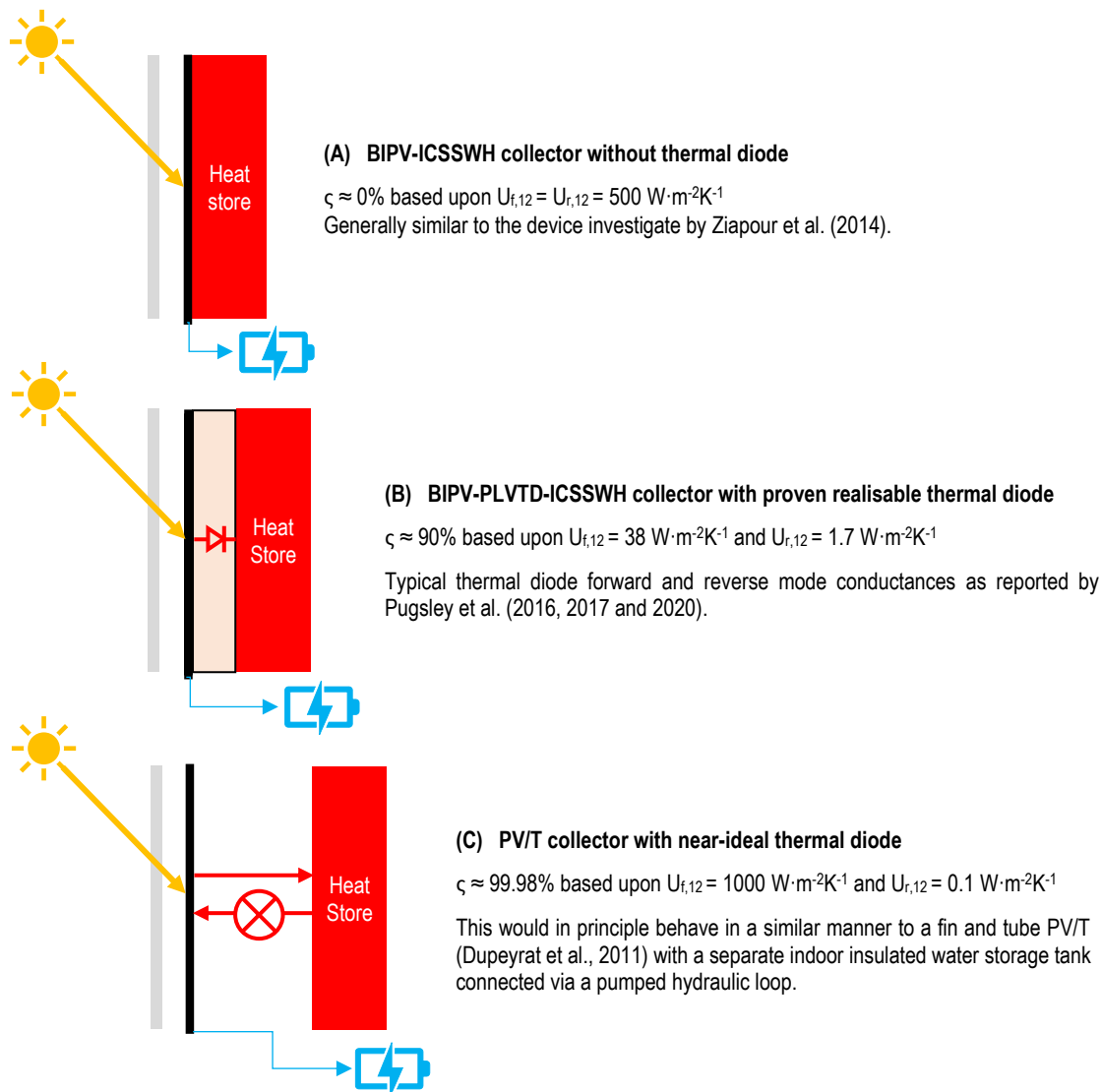


784
785
786

Figure 9: Dependence of overnight heat retention performance upon reverse mode thermal diode conductance

787 3.3 Behaviour in different climates

788 Figure 11 compares predicted behaviours of different BIPV-PLVTD-ICSSWH devices to
789 illustrate the overall influence of the PLVTD upon water storage tank temperature (T_3 ,
790 assumed fully mixed), diurnal thermal efficiency ($\eta_{T,24}$) and maximum power point
791 photovoltaic efficiency ($\eta_{E,mp}$) over a multi-day period without thermal load (ie no hot
792 water draw-offs). Results were calculated using Equations 5-10, 15-21, 32, 34 & 37
793 based upon the physical attributes described in Figure 1 and Table 3; a wind speed of
794 2 m/s; data for summertime average daily solar insolation on a vertical equator facing
795 surface in Rome ($H_{24}=12\text{MJ/m}^2$, see Table 1); and corresponding average ambient
796 temperatures of $T_a=25^\circ\text{C}$ during daytime and $T_a=19^\circ\text{C}$ at night (NASA, 2019). The
797 three modelled variants are summarised on Figure 10.



798

799 *Figure 11: Investigated model variants*

800

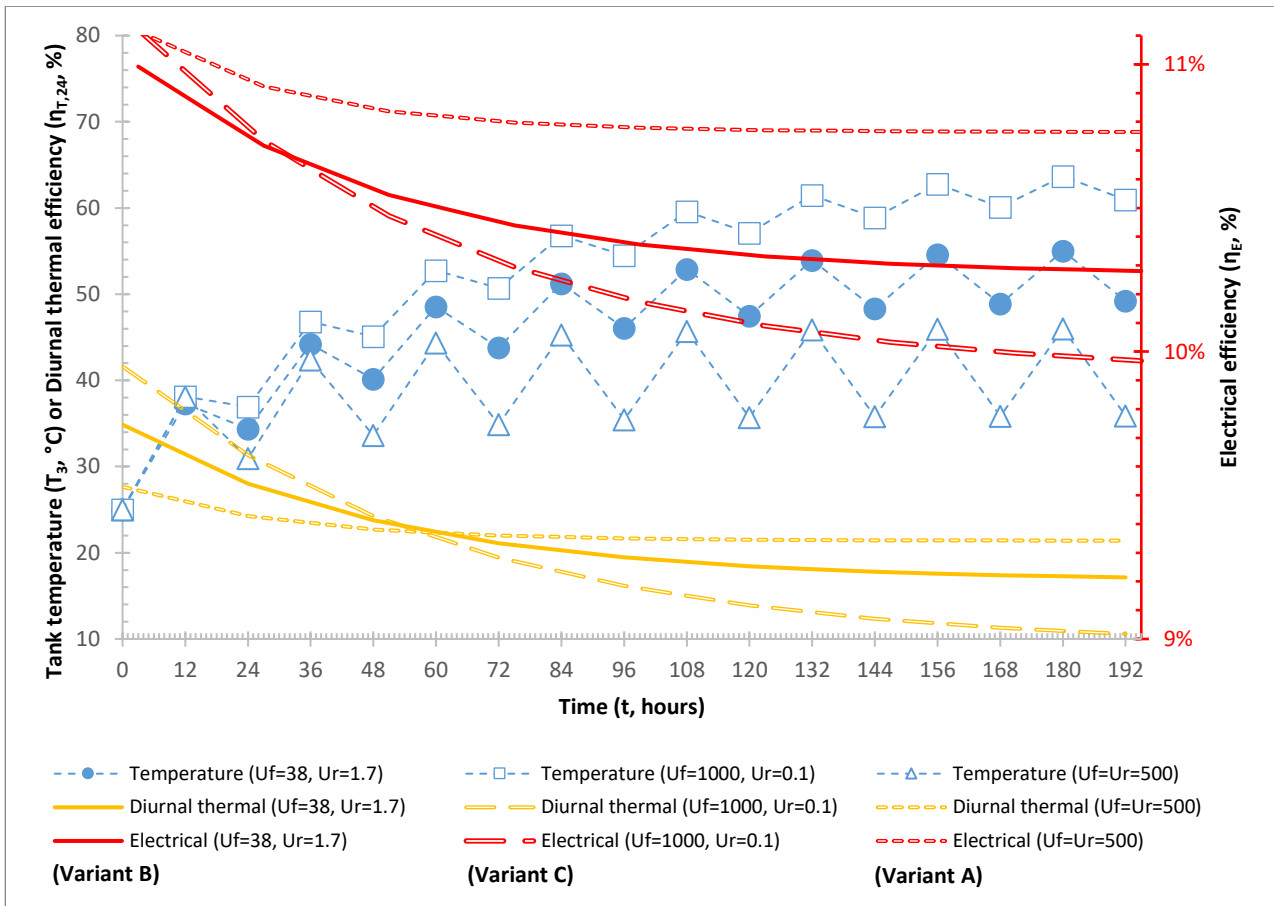
801 Figure 11 shows how tank temperatures (starting at $T_3=T_a=25^\circ\text{C}$) rise each day (solar
 802 collection) and fall each night (net heat losses) during an 8-day period of summertime
 803 stagnation (eg no thermal load due to a building being unoccupied during vacations).
 804 All three device variants achieve similar zero-loss solar thermal efficiencies ($\eta_T \approx 75\%$
 805 at $N=0 \text{ m}^2\text{K}\cdot\text{W}^{-1}$ as per Figure 7) and therefore also achieve similar maximum tank
 806 temperatures ($T_3 \approx T_a + 13 \approx 38^\circ\text{C}$) and average electrical efficiencies ($\eta_E \approx 11\%$) during
 807 Day 1. However, their differing overnight heat loss coefficients result in differing tank
 808 temperatures by dawn the next day, which causes differences in overall Day 1 diurnal
 809 thermal efficiencies ($\eta_{T,24} = \eta_{T,col} \cdot \eta_{T,ret}$) such that the conventional PV/T with separate
 810 tank performs best (Variant C: $\eta_{T,24} = 42\%$), the BIPV-ICSSWH without thermal diode
 811 performs worst (Variant A: $\eta_{T,24} = 28\%$) and the BIPV-PLVTD-ICSSWH achieves a good
 812 compromise (Variant B: $\eta_{T,24} = 35\%$). After 8 days stagnation, tank temperatures have

813 risen to $T_3=46^\circ\text{C}$, 55°C and 64°C for Variants A, B and C respectively. Consequently,
814 in terms of Day 8 performances, the conventional PV/T with separate tank performs
815 worst (Variant C: $\eta_{T,24}=10.6\%$ and $\eta_E\approx 10.0\%$) and the BIPV-ICSSWH without thermal
816 diode performs best (Variant A: $\eta_{T,24}=21.4\%$ and $\eta_E\approx 10.8\%$). The device with the
817 BIPV-PLVTD-ICSSWH again achieves a compromise (Variant B: $\eta_{T,24}=17.1\%$ and
818 $\eta_E\approx 10.3\%$). Figure 11 results were calculated based on average summer conditions
819 for a south facing wall in Rome. In practice, the ambient temperatures and insolation
820 levels during a particularly hot and sunny period could be considerably higher than
821 average, and those typically occurring during winter would be notably lower.

822 Dupeyrat et al. (2011) suggest that 85°C is an appropriate maximum temperature
823 limit for PV/T absorbers constructed using conventional Ethylene Vinyl Acetate (EVA)
824 lamination techniques. Calculations based on $H_{24}=20\text{MJ/m}^2$, $T_a=35^\circ\text{C}$ during daytime,
825 and $T_a=25^\circ\text{C}$ at night, and no wind, suggest that maximum summertime tank and
826 absorber stagnation temperatures could reach a potentially damaging $T_3\approx T_0\approx 106^\circ\text{C}$ in
827 the case of a conventional PV/T (Variant C) but would be maintained at a lower and
828 safer maximum temperature of $T_3\approx T_0\approx 86^\circ\text{C}$ in the case of the BIPV-PLVTD-ICSSWH
829 (Variant B) and would reach only $T_3\approx T_0\approx 67^\circ\text{C}$ in the case of a simple BIPV-ICSSWH
830 without PLVTD (Variant A). This clearly demonstrates the benefit of the BIPV-ICSSWH
831 concept in respect of minimising stagnation temperatures. In practice, conventional
832 PV/T systems require continuous pumping of heat transfer fluid from the collector to
833 the tank during sunny periods, otherwise much higher absorber stagnation
834 temperatures will occur ($T_0>150^\circ\text{C}$). Inherent electricity demands to run pumps would
835 significantly reduce net electrical yields. By contrast, a BIPV-ICSSWH or BIPV-PLVTD-
836 ICSSWH approach does not require pumps to operate when there is no thermal
837 demand, hence the net electrical yield would be higher than for conventional PV/T.

838 Calculations for a typical winter scenario in Rome based on $H_{24}=12.4\text{MJ/m}^2$ (see
839 Table 1), $T_a=14^\circ\text{C}$ during daytime, and $T_a=8^\circ\text{C}$ at night, and 5m/s wind, suggest that
840 the Day 1 diurnal thermal efficiency of a BIPV-PLVTD-ICSSWH (Variant B: $\eta_{T,24}=30\%$)
841 would be notably better than that of a BIPV-ICSSWH without PLVTD (Variant A:
842 $\eta_{T,24}=21\%$), although slightly worse than for conventional PV/T (Variant C: $\eta_{T,24}=38\%$).
843 This clearly demonstrates the benefit of incorporating a PLVTD to reduce overnight
844 heat losses and thus make heat available during the night and early morning hours.

845



846
847 *Figure 11: Comparison of tank temperature, diurnal thermal efficiency, and electrical efficiency over a multi-day period*
848

849 **4 Conclusions**

850 This two-part study examines an alternative space-and-energy-efficient approach to
851 BIPV/T which combines BIPV, ICSSWH, and PLVTD concepts. This paper (Part 1 of 2)
852 has reviewed the state-of-the-art for each of the technologies and established the
853 following benchmark performance targets:

- 854
- Solar thermal efficiency $\eta_{T,col} \approx 60\%$ at $N \approx 0.035 \text{ m}^2 \text{ K} \cdot \text{W}^{-1}$ and 2m/s wind speed.
 - Heat loss coefficients of $U_{r,sys} A_{sys} / A_1 \approx 1 \text{ W} \cdot \text{m}^{-2} \text{ K}^{-1}$ and $U_{r,sys} A_{sys} / u \approx 10 \text{ W} \cdot \text{m}^{-3} \cdot \text{K}^{-1}$ at
856 $\Delta T_{3a} \approx 25^\circ \text{C}$ and 2m/s wind speed.
 - PV/T performance ratios (relative to an ideal PV/T collector) of $PR_{T3} = 85\%$ and
858 $PR_{T3} = 75\%$ for uncovered and covered collectors respectively.

859 A heat transfer model of a BIPV-PLVTD-ICSSWH façade element was developed to
860 enable solar thermal collection, photovoltaic generation, and overnight heat retention
861 behaviours to be evaluated under various operating scenarios. Subsequent work
862 (presented in Part 2 of 2 of this study) provides experimental validation of the model.
863 The model was interrogated based on notional $A_1 = 1 \text{ m}^2$ solar absorber area, 75% PV

864 cell coverage, and $u=100\text{L}$ storage tank to examine how electrical and thermal
865 performances are influenced by PLVTD diodicity characteristics. Key findings can be
866 summarized as follows:

- 867 • Increasing forward mode PLVTD thermal conductance improves solar thermal
868 and photovoltaic performances. The degree of improvement gained is dependent
869 upon operating conditions such as irradiance, ambient temperature, heat
870 delivery temperature, wind speed and electrical load.
- 871 • Benchmark PV and solar thermal collection targets are achievable if the PLVTD
872 achieves $U_{f,12} > 500 \text{ W}\cdot\text{m}^{-2}\text{K}^{-1}$ and PV cell coverage is $>90\%$, although there is
873 only minimal benefit ($<2\%$) to be gained by increasing forward mode diode
874 thermal conductance above the knee value of $U_{f,12} \approx 100 \text{ W}\cdot\text{m}^{-2}\text{K}^{-1}$. Lower PLVTD
875 conductances impair absorber-to-tank heat transfer causing high absorber
876 temperatures which increase heat and electrical losses.
- 877 • Reducing reverse mode PLVTD thermal conductance improves overnight heat
878 retention performance. Achieving the target benchmark would require
879 $U_{r,12} < 0.5 \text{ W}\cdot\text{m}^{-2}\text{K}^{-1}$. Excessive heat losses and vulnerability to wind worsen
880 significantly above a notional threshold of $U_{r,12} \approx 2 \text{ W}\cdot\text{m}^{-2}\text{K}^{-1}$, especially when the
881 absorber is exposed (no cover).

882 The model was used to predict the multi-day period behaviour of various BIPV-PLVTD-
883 ICSSWH design and operating scenario variants, without thermal load. Key findings
884 can be summarized as follows:

- 885 • During summertime in Rome (insolation $H_{24}=12\text{MJ}/\text{m}^2$, wind speed 2 m/s ,
886 ambient temperatures $T_a=25^\circ\text{C}$ daytime and $T_a=19^\circ\text{C}$ at night) diurnal thermal
887 efficiency of $\eta_{T,24}=35\%$ and average photovoltaic efficiency of $\eta_E \approx 11\%$ are
888 predicted for the base case PLVTD ($U_{f,12}=38 \text{ W}\cdot\text{m}^{-2}\text{K}^{-1}$ and $U_{r,12}=1.7 \text{ W}\cdot\text{m}^{-2}\text{K}^{-1}$).
889 Solar thermal and photovoltaic performances are minimally sensitive to changes
890 in forward mode PLVTD conductance in the range $38 < U_{f,12} < 1000 \text{ W}\cdot\text{m}^{-2}\text{K}^{-1}$.
- 891 • Under particularly hot and sunny conditions (insolation $H_{24}=20\text{MJ}/\text{m}^2$, no wind,
892 ambient temperatures $T_a=35^\circ\text{C}$ daytime and $T_a=25^\circ\text{C}$ at night) the model
893 predicts that the base case BIPV-PLVTD-ICSSWH would limit maximum tank and
894 absorber stagnation temperatures to $T_3 \approx T_0 \approx 86^\circ\text{C}$ without the need to operate
895 fluid circulation pumps whereas a conventional PV/T system could reach a
896 potentially damaging $T_3 \approx T_0 \approx 106^\circ\text{C}$ and would require pumps to be energised

897 continuously during collection periods to prevent even higher ($T_0 > 150^\circ\text{C}$)
898 temperatures developing.

899 • Overnight heat retention is very sensitive to changes in reverse mode PLVTD
900 conductance such that increasing or decreasing in the range
901 $0.1 < U_{r,12} < 500 \text{ W}\cdot\text{m}^{-2}\text{K}^{-1}$ changes diurnal thermal efficiency by $\pm 7\%$ relative to
902 the base case ($U_{r,12} = 1.7 \text{ W}\cdot\text{m}^{-2}\text{K}^{-1}$). Pronounced heat losses occur during winter
903 in the $U_{r,12} 500 \text{ W}\cdot\text{m}^{-2}\text{K}^{-1}$ case owing to low ambient temperatures and increased
904 wind speeds and become very reliant on the insulation provided by the
905 transparent cover.

906 The passive BIPV-PLVTD-ICSSWH approach to controlling overheating significantly
907 reduces the risk of stagnation damage and increases net electrical yields compared to
908 conventional BIPV/T approaches. This alternative approach to BIPV/T could have
909 positive impacts in the context of realising NZEBs as part of global efforts to tackle the
910 climate crisis.

911 **Acknowledgements**

912 This research was enabled in its early stages by studentship funding support from the
913 Northern Ireland Department for the Economy. The work was subsequently progressed
914 with funding support from SolaForm Ltd and was completed as part of the
915 "SolaNetwork" project funded by the UKRI Engineering and Physical Sciences Research
916 Council (EP/T004819/1). The authors would also like to thank networking support
917 funded by the European Union FP7 COST Action TU1205 "Building Integration of Solar
918 Thermal Systems".

919 **Nomenclature**

920 *Latin symbols*

921	A	Surface area [m^2]
922	c_p	Specific heat capacity at constant pressure [$\text{J}\cdot\text{kg}^{-1}\text{K}^{-1}$]
923	FF	Photovoltaic Fill Factor [%]
924	G	Solar irradiance [$\text{W}\cdot\text{m}^{-2}$]
925	H	Solar insolation [$\text{MJ}\cdot\text{m}^{-2}$]
926	I	Electrical current [A]
927	k	Thermal conductivity [$\text{W}\cdot\text{m}^{-1}\text{K}^{-1}$]
928	K	Photovoltaic performance correction coefficients [% or %/K]
929	m	Mass [kg]
930	M	Mass flow rate [$\text{kg}\cdot\text{s}^{-1}$]
931	N	Solar Thermal Condition [$\text{m}^2\cdot\text{K}\cdot\text{W}^{-1}$]
932	q	Thermal or electrical power [W]
933	$Q_{[t]}$	Thermal energy, cumulative during time period [MJ]

934	PR	Performance ratio [%]
935	R	Thermal or electrical resistance [$K \cdot W^{-1}$]
936	t	Time [s]
937	T	Temperature [$^{\circ}C$]
938	$\bar{T}_{[t]}$	Average temperature, during time period [$^{\circ}C$]
939	u	Volume [m^3]
940	U	Thermal conductance or heat transfer coefficient [$W \cdot m^{-2} K^{-1}$]
941	V	Electrical voltage [V]
942	x	Distance along an axis which is parallel to the PLVTD depth [m]
943	y	Distance along horizontal axis perpendicular to PLVTD depth [m]
944	z	Distance along an axis which is perpendicular to x and y axes [m]
945		

946 **Greek and other symbols**

947	α	Absorptivity
948	ε	Emissivity
949	ΔT	Temperature difference [$^{\circ}C$]
950	η	Efficiency [%]
951	ζ	Diodicity [%]
952	τ	Transmissivity
953		

954 **Subscripts**

955	0	Photovoltaic cells
956	1	Planar Liquid-Vapour Thermal Diode, Plate 1 which is the evaporator in forward mode
957	2	Planar Liquid-Vapour Thermal Diode, Plate 2 which is the condenser on forward mode
958	3	Hot water storage tank
959	4	Sidewalls of the Planar Liquid-Vapour Thermal Diode
960	5	External surface of the solar absorber
961	6	Transparent element covering solar absorber
962	0a	Between PV cells and ambient environment
963	03	Between PV cells and hot water storage tank
964	1a	Between solar absorber and ambient environment
965	12	Between (or average of) the two plates
966	15	Between the PLVTD and the external surface of the solar absorber (through the laminate)
967	23	Between the PLVTD and the water storage tank
968	24	Diurnal period of 24 hours
969	3a	Between water storage tank and ambient environment
970	3ia	Between water storage tank and ambient environment through insulation
971	365	Annual period of 365 days
972	4a	Between PLVTD sidewalls and ambient environment
973	56	Across the air gap between the solar absorber and transparent cover
974	6a	Between the transparent cover and the ambient environment
975	a	Ambient environment
976	avg	Average
977	col	Collection (period of solar absorber illumination, eg daytime)
978	E	Electrical
979	f	Forward mode
980	h	Horizontal orientation

981	inst	Instantaneous
982	L	Loss to ambient environment
983	load	Applied electrical load
984	mpp	Maximum Power Point
985	oc	Open circuit
986	P	Pump
987	PV	Photovoltaic
988	r	Reverse mode
989	ret	Retention (period without solar absorber illumination, eg night-time)
990	sc	Short circuit
991	STC	At Standard Test Conditions
992	sys	Whole system
993	T	Thermal
994	T3	At the hot water storage tank temperature
995	I:T	Current-Temperature relationship
996	V:T	Voltage-Temperature relationship
997	V:G	Voltage-Irradiance relationship
998		

999 **Abbreviations**

1000	a-si	Amorphous silicon
1001	BIPV	Building Integrated PhotoVoltaics
1002	BISTS	Building Integrated Solar Thermal Systems
1003	CdTe	Cadmium Telluride
1004	CIGS	Copper Indium Gallium Selenium
1005	ICSSWH	Integrated Collector-Storage Solar Water Heater
1006	mc-si	Mono-crystalline silicon
1007	NZEB	Net Zero Energy Building
1008	pc-si	Poly-crystalline silicon
1009	PLVTD	Planar Liquid-Vapour Thermal Diode
1010	PV/T	Photovoltaic-Thermal

1011 **References**

- 1012 Abdelrazik, A., Al-Sulaiman, F., Saidur, R., Ben-Mansour, R. (2018). A review on recent development for the design and packaging
1013 of hybrid photovoltaic/thermal (PV/T) solar systems. *Renewable and Sustainable Energy Reviews* 95 (2018) 110–129
- 1014 Amerongen, G., Lee, J., Suter, J. (2013). Legionella and solar water heaters. Report commissioned by the Solar Certification Fund.
1015 Available at: <www.estif.org/solarkeymarknew/images/downloads/SCF/scfdeliverables/Report%20SCF%20Legionella%20and%20solar%20water%20heaters%20%20Final%202013%2004.pdf>
1016
- 1017 Barone, G., Buonomano, A., Forzano, C., Palombo, A., Panagopoulos, O. (2019). Photovoltaic thermal collectors: Experimental
1018 analysis and simulation model of an innovative low-cost water-based prototype. *Energy* 179 (2019) 502-516
- 1019 Beausoleil-Morrison, I., Kemery, B., Wills, A., Meister, C. (2019). Design and simulated performance of a solar-thermal system
1020 employing seasonal storage for providing the majority of space heating and domestic hot water heating needs to a single-family
1021 house in a cold climate. *Solar Energy* 191 (2019) 57–69
- 1022 Belussi, L., Barozzi, B., Bellazzi, A., Danza, L., Devitofrancesco, A., Fanciulli, C., Ghellere, M., Guazzi, G., Meroni, I., Salamone, F.,
1023 Scamoni, F., Scrosati, C. (2019). A review of performance of zero energy buildings and energy efficiency solutions. *Journal of Building
1024 Engineering* 25 (2019) 100772
- 1025 Besheer, A., Smyth, M., Zacharopoulos, A., Mondol, J., Pugsley, A. (2016). Review on recent approaches for hybrid PV/T solar
1026 technology. *International Journal of Energy Research*. DOI: 10.1002/er.3567
- 1027 Bilardo, M., Fraise, G., Pailha, M., Fabrizio, E. (2019). Modelling and performance analysis of a new concept of integral collector
1028 storage (ICS) with phase change material. *Solar Energy* 183 (2019) 425–440

- 1029 Borello, D., Corsini, A., Delibra, G., Evangelisti, S., Micangeli, A. (2012). Experimental and computational investigation of a new solar
1030 integrated collector storage system. *Applied Energy* 97 (2012) 982–989
- 1031 Boreyko, J. & Chen, C. (2013). Vapor chambers with jumping-drop liquid return from superhydrophobic condensers. *International*
1032 *Journal of Heat and Mass Transfer* 61 (2013) 409–418
- 1033 Bosch (2010). High performance – Stable yields. Bosch Solar Cell M 2BB. [Last accessed: 10 September 2016]. Arnstadt, Germany:
1034 Bosch Solar Energy AG. Available at: <<http://www.bosch-solarenergy.com>>.
- 1035 Buonomano, A., Calise, F., Palombo, A., Vicidomini, M. (2016). BIPVT systems for residential applications: An energy and economic
1036 analysis for European climates. *Applied Energy* 184 (2016) 1411–1431
- 1037 Calise, F., d'Accadia, M, Figaj, R., Vanoli, L., (2016). A novel solar-assisted heat pump driven by photovoltaic/thermal collectors:
1038 Dynamic simulation and thermoeconomic optimization. *Energy* 95, 346-66
- 1039 Chaabane, M., Mhiri, H., Bournot, P. (2014). Thermal performance of an integrated collector storage solar water heater (ICSSWH)
1040 with phase change materials (PCM). *Energy Conversion and Management* 78 (2014) 897–903.
- 1041 COST Action TU1205 (2015). Overview of BISTS state of the art, models and applications. ISBN: 978-9963-697-16-8. Cyprus
1042 University of Technology / European Union Horizon 2020.
- 1043 Das, D., Kalita, P., Roy, O. (2018). Flat plate hybrid photovoltaic- thermal (PV/T) system: A review on design and development.
1044 *Renewable and Sustainable Energy Reviews* 84 (2018) 111–130
- 1045 De Beijer, H. (1998). Product development in solar water heating. *Renewable Energy* 5 (1998) 201-204
- 1046 Deng, J., O'Donovan, T., Tian, Z., King, J., Speake, S. (2019). Thermal performance predictions and tests of a novel type of flat plate
1047 solar thermal collectors by integrating with a freeze tolerance solution. *Energy Conversion and Management* 198 (2019) 111784
- 1048 DGS - Deutsche Gesellschaft für Sonnenenergie (2008). Planning and Installing Photovoltaic Systems - A guide for installers,
1049 architects and engineers. 2nd ed. London: Earthscan. ISBN-13: 978-1-84407-442-6
- 1050 Drosou, V., Tsekouras, P., Oikonomou, T., Kosmopoulos, P., Karytsas, C. (2014). The HIGH-COMBI project: High solar fraction heating and
1051 cooling systems with combination of innovative components and methods. *Renewable and Sustainable Energy Reviews* 29 (2014) 463–472
- 1052 Dupeyrat, P., Menezo, C., Rommel, M., Henning, H. (2011). Efficient single glazed flat plate photovoltaic-thermal hybrid collector for
1053 domestic hot water systems. *Solar Energy* 85, 1457-68
- 1054 Eames, P. and Griffiths, P. (2006). Thermal behaviour of integrated solar collector/storage unit with 65C phase change material. *Energy*
1055 *Conversion and Management* 47 (2006) 3611–3618
- 1056 Faiman, D., Hazan, H. and Laufer, I. (2001). Reducing the Heat Loss at Night from Solar Water Heaters of the Integrated Collector-
1057 Storage Variety. *Solar Energy*, 71 (2) 87-93
- 1058 Fuentes, M., Vivar, M., Casab, J., Aguilera, J. (2018). An experimental comparison between commercial hybrid PV-T and simple PV
1059 systems intended for BIPV. *Renewable and Sustainable Energy Reviews* 93 (2018) 110–120
- 1060 Garnier, C., Currie, J., Muneer, T. (2009). Integrated collector storage solar water heater: Temperature stratification. *Applied Energy*
1061 86 (2009) 1465–1469
- 1062 Good, C., Andresen, I., Hestnes, A. (2015). Solar energy for net zero energy buildings – A comparison between solar thermal, PV
1063 and photovoltaic-thermal (PV/T) systems. *Solar Energy* 122, 986–96
- 1064 Guarracino, I., Freeman, J., Ramos, A., Kalogirou, S., Ekins-Daukes, N., Markides, C. (2019). Systematic testing of hybrid PV-thermal
1065 (PVT) solar collectors in steady-state and dynamic outdoor conditions. *Applied Energy* 240 (2019) 1014–1030
- 1066 Harmim, A., Boukar, M., Amar, M., Haida, A. (2019). Simulation and experimentation of an integrated collector storage solar water
1067 heater designed for integration into building façade. *Energy* 166 (2019) 59-71
- 1068 IEA – International Energy Agency (2018). Key World Energy Statistics 2018. Paris, France: IEA.
- 1069 IEA/UN - International Energy Agency and the United Nations Environment Programme (2018). 2018 Global Status Report: towards
1070 a zero-emission, efficient and resilient buildings and construction sector. Paris, France: IEA for the Global Alliance for Buildings and
1071 Construction (GlobalABC). ISBN: 978-92-807-3729-5.
- 1072 Kalogirou, S. (2009). Solar energy engineering. London: Academic Press (Elsevier) ISBN 13: 978-0-12-374501-9
- 1073 Kats, G., Seal, A. (2012). Buildings as Batteries: The Rise of 'Virtual Storage'. *The Electricity Journal* 25 (10) 59-70
1074 <http://dx.doi.org/10.1016/j.tej.2012.11.004>
- 1075 Krauter, S. (2004). Development of an integrated solar home system. *Solar Energy Materials & Solar Cells* 82 (2004) 119–130
- 1076 Li, S., Zhang, Y., Zhang, K., Li, X., Li, Y., Zhang, X. (2013). Study on performance of storage tanks in solar water heater system in
1077 charge and discharge progress (SHC 2013, International Conference on Solar Heating and Cooling for Buildings and Industry).
1078 *Energy Procedia* 48 (2014) 384–393 doi: 10.1016/j.egypro.2014.02.045
- 1079 Li, X., Lin, A., Young, C., Dai, Y., Wang, C. (2019). Energetic and economic evaluation of hybrid solar energy systems in a residential
1080 net-zero energy building. *Applied Energy* 254 (2019) 113709

- 1081 Mehdaoui, F., Hazami, M., Messaouda, A., Guizani, A. (2019). Performance analysis of two types of Solar Heating Systems used in
1082 buildings under typical North-African climate (Tunisia). *Applied Thermal Engineering (AIP)*
1083 <https://doi.org/10.1016/j.applthermaleng.2019.114203>
- 1084 Michael, J., Iniyan, S., Goic, R. (2015). Flat plate solar photovoltaic–thermal (PV/T) systems. *Renewable & Sustainable Energy Reviews*
1085 51, 62–88
- 1086 Mohamad, A. (1997). Integrated Solar Collector-Storage Tank System with Thermal Diode. *Solar Energy* 61 (3) 211-218
- 1087 Muhumuza, R., Zacharopoulos, A., Mondol, J., Smyth, M. (2019a). Experimental study of heat retention performance of thermal diode
1088 Integrated Collector Storage Solar Water Heater (ICSSWH) configurations. *Sustainable Energy Technologies and Assessments* 34
1089 (2019) 214–219
- 1090 Muhumuza, R., Zacharopoulos, A., Mondol, J., Smyth, M., Pugsley, A., Giuzio, G., Kurmis, D. (2019b). Experimental investigation of
1091 horizontally operating thermal diode solar water heaters with differing absorber materials under simulated conditions. *Renewable*
1092 *Energy*, Volume 138, August 2019, Pages 1051-1064
- 1093 Muhumuza, R., Zacharopoulos, A., Mondol, J., Smyth, M., Pugsley, A., McGee, J. (2020). Simulation and experimental validation of
1094 solar radiation distribution on the absorber of a line-axis asymmetric compound parabolic concentrator. *Solar Energy* 198 (2020) 36-
1095 52. <https://doi.org/10.1016/j.solener.2020.01.033>.
- 1096 NASA - National Aeronautics and Space Administration (2019). Data Access Viewer for Prediction of Worldwide Energy Resource
1097 (POWER) Project funded through the NASA Earth Science/Applied Science Program. Hampton, USA: Langley Research Center
1098 (LaRC). Available at: < <https://power.larc.nasa.gov/data-access-viewer/> > [Last accessed: 07/10/19].
- 1099 O'Hegarty, R., Kinnane, O., McCormack, S. (2014). A Case for façade located solar thermal collectors. (International Conference on
1100 Solar Heating and Cooling for Buildings and Industry, SHC 2014). *Energy Procedia* 70 (2015) 103–110 doi:
1101 10.1016/j.egypro.2015.02.104
- 1102 Pugsley, A., Mondol, J., Smyth, M., Zacharopoulos, A., Di Mattia, L. (2016). Experimental characterisation of a flat panel integrated
1103 collector-storage solar water heater featuring a photovoltaic absorber and a planar liquid-vapour thermal diode. *Proceedings of 11th*
1104 *ISES EuroSun Conference: Palma (Mallorca), Spain from 11 to 14 October 2016*. Martinez, V. & Gonzalez, J. (eds.).
- 1105 Pugsley, A. (2017). Theoretical and experimental analysis of a novel flat photovoltaic-thermal solar water heater with integrated
1106 energy storage via a planar liquid-vapour thermal diode. Ulster University PhD Thesis (uk.bl.ethos.713462) published July 2017.
- 1107 Pugsley, A., Zacharopoulos, A., Mondol, J., Smyth, M. (2019). Theoretical and experimental analysis of a horizontal Planar Liquid-
1108 Vapour Thermal Diode (PLVTD). *International Journal of Heat and Mass Transfer* 144 (2019) 11866
- 1109 Pugsley, A., Zacharopoulos, A., Mondol, J., Smyth, M. (2020). Vertical Planar Liquid-Vapour Thermal Diodes (PLVTD) and their
1110 application in building façade energy systems. *Applied Thermal Engineering* (submitted for publication 01/2020, under review)
- 1111 Qu, M., Chen, J., Nie, L., Li, F., Yu, Q., Wang, T. (2016). Experimental study on the operating characteristics of a novel
1112 photovoltaic/thermal integrated dual-source heat pump water heating system. *Applied Thermal Engineering* 94, 819–26
- 1113 Quinlan, P. (2010). The Development of a Novel Integrated Collector Storage Solar Water Heater (ICSSWH) Using Phase Change
1114 Materials and Partial Evacuation. PhD Thesis, University of Ulster.
- 1115 Rhee, J., Campbell, A. Mariadass, A., Morhous, B. (2010). Temperature stratification from thermal diodes in solar hot water storage
1116 tank. *Solar Energy* 84 (2010) 507–511
- 1117 Santbergen, R., Rindt, C., Zondag, H., Van Zolingen, R. (2010). Detailed analysis of the energy yield of systems with covered sheet-
1118 and-tube PVT collectors. *Solar Energy* 84, 867–78.
- 1119 Saretta, E., Bonomo, P., Frontini, F. (2020). A calculation method for the BIPV potential of Swiss façades at LOD2.5 in urban areas:
1120 A case from Ticino region. *Solar Energy* 195 (2020) 150–165
- 1121 Schmidt, C. and Goetzberger, A. (1990). Single-Tube Integrated Collector Storage Systems with Transparent Insulation and Involute
1122 Reflector. *Solar Energy* 45 (2) 93-100
- 1123 Singh, R., Lazarus, I., Souliotis, M. (2016). Recent developments in integrated collector storage (ICS) solar water heaters: A review.
1124 *Renewable & Sustainable Energy Reviews* 54, 270-98
- 1125 Smyth, M., Eames, P., Norton, B. (1999). A comparative performance rating for an integrated solar collector/storage vessel with inner
1126 sleeves to increase heat retention. *Solar Energy* 66 (4) 291–303.
- 1127 Smyth, M., Eames, P., Norton, B. (2003). Heat Retaining Integrated Collector/Storage Solar Water Heaters. *Solar Energy* 75 (2003)
1128 27-34
- 1129 Smyth, M., McGarrigle, P., Eames, P., Norton, B. (2005). Experimental comparison of alternative convection suppression
1130 arrangements for concentrating integral collector storage solar water heaters. *Solar Energy* 78 (2005) 223–233
- 1131 Smyth, M., Eames, P. and Norton, B. (2006). Integrated Collector Storage Solar Water Heaters. *Renewable and Sustainable Energy*
1132 *Review* 10 (6) 503-538
- 1133 Smyth, M. (2015a). A solar water heater. Patent WO2010052010 held by Ulster University.

- 1134 Smyth, M., Besheer, A., Zacharopoulos, A., Mondol, J., Pugsley, A., Novaes, M. (2015b). Experimental evaluation of a Hybrid
1135 Photovoltaic/Solar Thermal (HyPV/T) Façade Module. Proceedings EURO ELECS Conference 21-23 July 2015, Guimarães, Portugal.
- 1136 Smyth, M., Quinlan, P., Mondol, J., Zacharopoulos, A., McLarnon, D., Pugsley, A. (2017). The evolutionary thermal performance &
1137 development of a novel thermal diode pre-heat solar water heater under simulated heat flux conditions. *Renewable Energy* 113
1138 (2017) 1160-1167
- 1139 Smyth, M., Quinlan, P., Mondol, J., Zacharopoulos, A., McLarnon, D., Pugsley, A. (2018). The experimental evaluation and improvements
1140 of a novel thermal diode pre-heat solar water heater under simulated solar conditions. *Renewable Energy* 121 (2018) 116-122
- 1141 Smyth, M., Pugsley, A., Hanna, G., Zacharopoulos, A., Besheer, A., Savvides, A. (2019). Experimental performance characterisation
1142 of a Hybrid Photovoltaic/Solar Thermal Façade module compared to a flat Integrated Collector Storage Solar Water Heater module.
1143 *Renewable Energy* 137 (2019) 137-143
- 1144 Sopian, K., Syahri, M., Abdullah, S., Othman, M., Yatim, B. (2004). Performance of a non-metallic unglazed solar water heater with
1145 integrated storage system. *Renewable Energy* 29 (2004) 1421–1430
- 1146 Souliotis, M., Quinlan, P., Smyth, M., Tripanagnostopoulos, Y., Zacharopoulos, A., Ramirez, M., Yianoulis, P. (2011). Heat retaining
1147 integrated collector storage solar water heater with asymmetric CPC reflector. *Solar Energy* 85 (2011) 2474–87
- 1148 Souliotis, M., Chemisana, D., Caouris, Y., Tripanagnostopoulos, Y. (2013). Experimental study of integrated collector storage solar
1149 water heaters. *Renewable Energy* 50 (2013) 1083-1094
- 1150 Souliotis, M., Papaefthimiou, S., Caouris, Y., Zacharopoulos, A., Quinlan, P., Smyth, M. (2017). Integrated collector storage solar
1151 water heater under partial vacuum. *Energy* 139 (2017) 991-1002
- 1152 Stackhouse, P., Zhang, T., Westberg, D., Barnett, A., Bristow, T., Macpherson, B., Hoell, J. (2018). POWER Release 8.0.1 (with GIS
1153 Applications) Methodology, Data Parameters, Sources, & Validation. Data Version 8.0.1. Web Site Version 1.1.0. Hampton, USA:
1154 NASA LaRC, Langley Research Center.
- 1155 Sultan, S., Efzan, E. (2018). Review on recent Photovoltaic/Thermal (PV/T) technology advances and applications. *Solar Energy*
1156 173 (2018) 939–954
- 1157 Tian, M., Yu, X., Su, Y., Zheng, H., Riffat, S. (2019). A study on incorporation of transpired solar collector in a novel multifunctional
1158 PV/Thermal/Daylighting (PV/T/D) panel. *Solar Energy* 165 (2018) 90–99
- 1159 Tripanagnostopoulos, Y., Souliotis, M., Nousia, T. (2002). CPC type collector storage systems. *Solar Energy* 72 (4) 327-350
- 1160 Tripanagnostopoulos, Y., Souliotis, M. (2006). ICS Solar Systems with Two Water Tanks. *Renewable Energy* 29 (1) 13-38
- 1161 Twidell, J. & Weir, T. (2006). *Renewable Energy Resources* (2nd ed.) London: Taylor Francis. ISBN13:9-78-0-419-25330-3
- 1162 Yang, T., Athienitis, A. (2016). A review of research and developments of building-integrated photovoltaic/thermal (BIPV/T) systems.
1163 *Renewable and Sustainable Energy Reviews* 66 (2016) 886–912
- 1164 Ziapour, B., Palideh, V., Mohammadnia, A. (2014). Study of an improved integrated collector-storage solar water heater combined
1165 with the photovoltaic cells. *Energy Conversion and Management* 86 (2014) 587–594.
- 1166 Zondag, H. (2008). Flat-plate PV–thermal collectors and systems: a review. *Renewable & Sustainable Energy Reviews* 12, 891–959.